MCB
Journals.ASM.org

2-Deoxyglucose Impairs *Saccharomyces cerevisiae* Growth by Stimulating Snf1-Regulated and α-Arrestin-Mediated Trafficking of Hexose Transporters 1 and 3

Allyson F. O'Donnell,[a,b] Rhonda R. McCartney,[c] Dakshayini G. Chandrashekarappa,[c] Bob B. Zhang,[c] Jeremy Thorner,[b] Martin C. Schmidt[c]

Department of Cell Biology, University of Pittsburgh School of Medicine, Pittsburgh, Pennsylvania, USA[a]; Division of Biochemistry, Biophysics and Structural Biology, Department of Molecular and Cell Biology, University of California, Berkeley, California, USA[b]; Department of Microbiology and Molecular Genetics, University of Pittsburgh School of Medicine, Pittsburgh, Pennsylvania, USA[c]

The glucose analog 2-deoxyglucose (2DG) inhibits the growth of *Saccharomyces cerevisiae* and human tumor cells, but its modes of action have not been fully elucidated. Yeast cells lacking Snf1 (AMP-activated protein kinase) are hypersensitive to 2DG. Overexpression of either of two low-affinity, high-capacity glucose transporters, Hxt1 and Hxt3, suppresses the 2DG hypersensitivity of *snf1*Δ cells. The addition of 2DG or the loss of Snf1 reduces *HXT1* and *HXT3* expression levels and stimulates transporter endocytosis and degradation in the vacuole. 2DG-stimulated trafficking of Hxt1 and Hxt3 requires Rod1/Art4 and Rog3/Art7, two members of the α-arrestin trafficking adaptor family. Mutations in *ROD1* and *ROG3* that block binding to the ubiquitin ligase Rsp5 eliminate Rod1- and Rog3-mediated trafficking of Hxt1 and Hxt3. Genetic analysis suggests that Snf1 negatively regulates both Rod1 and Rog3, but via different mechanisms. Snf1 activated by 2DG phosphorylates Rod1 but fails to phosphorylate other known targets, such as the transcriptional repressor Mig1. We propose a novel mechanism for 2DG-induced toxicity whereby 2DG stimulates the modification of α-arrestins, which promote glucose transporter internalization and degradation, causing glucose starvation even when cells are in a glucose-rich environment.

Cells sense and respond to changes in the nutrient supply to ensure optimal cell growth and survival. To achieve this adaptation, cell-signaling cues dictate compensatory alterations in the transcriptome and proteome (1–5). The addition of the glucose analog 2-deoxyglucose (2DG) to cells causes a glucose starvation-like response, inhibiting growth and reducing viability even in the presence of abundant glucose (6, 7). 2DG is taken up and converted to 2-deoxyglucose-6-phosphate (2DG-6P) (8, 9); however, the absence of a hydroxyl group on C-2 prevents the further catabolism of 2DG-6P by phosphoglucose isomerase. Accumulation of 2DG-6P may result in product inhibition of hexokinase, thereby inhibiting glycolysis (10). In *Saccharomyces cerevisiae*, 2DG reportedly inhibits the biosynthesis of both cell wall polysaccharide and glycoprotein, causing cells to become osmotically fragile (11, 12). Whether these are the only means by which 2DG short-circuits normal glucose utilization remains unclear.

Addressing this question is of significant clinical importance, because 2DG is a potent inhibitor of cancer cell proliferation. 2DG impedes cancer progression in animal models and continues to be assessed as an anticancer therapeutic (13–16). 2DG selectively inhibits cancerous cells as a result of a key metabolic shift that distinguishes many malignant cells from the surrounding normal tissues. Many tumor cells shunt glucose through the glycolytic pathway and use lactic acid fermentation to generate ATP, a phenomenon first recognized by Otto Warburg (17, 18). In spite of the widespread use of 2DG, the mechanism by which it inhibits cell growth remains controversial; it has been reported to generate a dead-end metabolite in 2DG-6P that inhibits glycolytic flux, to reduce cellular ATP pools, and to impede proper protein glycosylation (6, 10, 19–21).

Yeast cells share metabolic similarities with cancerous cells in that they ferment glucose in the presence of oxygen and exhibit sensitivity to 2DG, even when glucose is available (7, 22). We have demonstrated that yeast cells lacking Snf1, the yeast ortholog of the catalytic subunit of mammalian AMP-activated protein kinase (AMPK), are hypersensitive to 2DG (7). Both Snf1 and mammalian AMPK respond to the cellular energy status, becoming activated as the ratio of AMP and ADP to ATP rises (23, 24). In yeast, active Snf1 is needed for cells to switch from using glucose to employing alternative carbon sources, such as sucrose or ethanol (25). In agreement with observations in mammalian cells (26, 27), treatment of yeast with 2DG increases Snf1 activity, as evidenced by increased phosphorylation of the conserved threonine in the activation loop (7). Surprisingly, certain downstream effectors of Snf1 that are phosphorylated in response to glucose limitation are not detectably phosphorylated by Snf1 in response to 2DG (7). These findings suggested that 2DG-stimulated Snf1 might be selectively targeted to previously uncharacterized downstream effectors. To identify these effectors, we screened a systematic overexpression library (28) for suppressors of the hypersensitivity of

Received 22 September 2014 **Returned for modification** 11 October 2014
Accepted 23 December 2014

Accepted manuscript posted online 29 December 2014

Citation O'Donnell AF, McCartney RR, Chandrashekarappa DG, Zhang BB, Thorner J, Schmidt MC. 2015. 2-Deoxyglucose impairs *Saccharomyces cerevisiae* growth by stimulating Snf1-regulated and α-arrestin-mediated trafficking of hexose transporters 1 and 3. Mol Cell Biol 35:939–955. doi:10.1128/MCB.01183-14.

Address correspondence to Martin C. Schmidt, mcs2@pitt.edu.

Copyright © 2015, American Society for Microbiology. All Rights Reserved.

doi:10.1128/MCB.01183-14

Downloaded from http://mcb.asm.org/ on February 22, 2015 by University of Pittsburgh HSLS

TABLE 1 Yeast strains

Strain	Genotype	Reference or source
BY4741	*MAT***a** *his3Δ1 leu2Δ0 LYS2 met15Δ0 ura3Δ0*	85
EN60	*MAT***a** *ecm21Δ*::G418 *csr2Δ*::G418 *bsd2Δ rod1Δ rog3Δ*::natMX *ygr068cΔ ldb19Δ aly1Δ aly2Δ ylr392cΔ::HIS3 his3Δ0 ura3Δ0 leu2Δ0*	42
MSY1212	*MAT***a** *ura3-52 leu2Δ1 his3Δ200*	This study
MSY1217	*MAT***a** *ura3-52 leu2Δ1 his3Δ200 snf1Δ10*	This study
MSY1226	*MATα ura3-52 leu2Δ1 his3Δ200 reg1Δ::HIS3*	This study
MSY1227	*MAT***a** *ura3-52 leu2Δ1 his3Δ200 reg1Δ::HIS3 snf1Δ10*	This study
MSY1282	*MAT***a** *ura3 leu2 his3 met15Δ0 rod1Δ::KAN rog3Δ::KAN*	This study
MSY1284	*MATα ura3 leu2 his3 snf1Δ10 rod1Δ::KAN rog3Δ::KAN*	This study
MSY1285	*MAT***a** *ura3 leu2 his3 rog3Δ::KAN*	This study
MSY1286	*MATα ura3 leu2 his3 lys2Δ0 met15Δ0 rod1Δ::KAN*	This study
MSY1287	*MAT***a** *ura3 leu2 his3 met15Δ0 snf1Δ10 rod1Δ::KAN*	This study
MSY1288	*MATα ura3 leu2 his3 lys2Δ0 snf1Δ10 rog3Δ::KAN*	This study
BY Hxt1-GFP	*MAT***a** *HXT1*-GFP::*LEU2 his3Δ1 leu2Δ0 LYS2 met15Δ0 ura3Δ0*	This study
BY Hxt3-GFP	*MAT***a** *HXT3*-GFP::*LEU2 his3Δ1 leu2Δ0 LYS2 met15Δ0 ura3Δ0*	This study
1217 Hxt3-GFP	*MAT***a** *ura3-52 leu2Δ1 his3Δ200 snf1Δ10 HXT3*-GFP::*LEU2*	This study
1226 Hxt3-GFP	*MATα ura3-52 leu2Δ1 his3Δ200 reg1Δ::HIS3 HXT3*-GFP::*LEU2*	This study
BY4742 Hxt3-GFP	*MATα ura3-52 leu2Δ1 his3Δ200 lys2Δ HXT3*-GFP::*HIS3MX6*	33
rsp5-1 Hxt3-GFP strain	*MATα rsp5-1 ura3-52 leu2Δ1 his3Δ200 lys2Δ HXT3*-GFP::*HIS3MX6*	33

*snf1*Δ cells to 2DG. In this way, we identified *HXT1* and *HXT3*, which encode the low-affinity, high-capacity hexose transporters responsible for glucose uptake from a glucose-rich environment (29–31), suggesting that the levels of Hxt1 and Hxt3 become rate-limiting for growth on glucose in *snf1*Δ cells challenged with 2DG.

We demonstrate here that the addition of 2DG inhibits the transcription of *HXT1* and *HXT3* and also downregulates Hxt1 and Hxt3 by stimulating their endocytosis and trafficking to the vacuole. Hxt1 and Hxt3 endocytosis in response to 2DG is consistent with recent studies showing that nutrient starvation also causes Hxt1 and Hxt3 endocytosis in a process that requires the ubiquitin ligase Rsp5 (32, 33). Rsp5, a member of the Nedd4 ubiquitin ligase family, has a well-established role in regulating the trafficking of nutrient permeases and transporters in response to environmental changes (34–36). Hxt1 and Hxt3, like many of the integral membrane proteins regulated by Rsp5, lack the PPXY motifs needed to recruit this ligase directly (35, 37). Members of a recently described family of trafficking adaptors conserved from yeast to humans—known as the α-arrestins or, alternatively, as arrestin-related trafficking adaptors (ARTs)—each contain PPXY motifs, bind Rsp5 (or its mammalian counterparts), and recruit the ubiquitin ligase to specific membrane cargos (27, 37–47). Two paralogous α-arrestins, Rod1/Art4 and Rog3/Art7, are required for 2DG-induced endocytosis and vacuolar trafficking of Hxt1 and Hxt3, and their Rsp5-binding motifs are needed for this process.

Collectively, our findings indicate that 2DG stimulates the endocytosis of Hxt1 and Hxt3 in an α-arrestin-dependent and Snf1-regulated manner. Moreover, given recent evidence that endocytosis of at least one mammalian glucose transporter (GLUT1) is under the control of an α-arrestin (thioredoxin-interacting protein [TXNIP]) and AMPK (27), our observations have important implications for better understanding of the mechanism of 2DG toxicity in cancer cell models.

MATERIALS AND METHODS

Yeast strains and growth conditions. All the yeast strains used in this study were derived from the S228C lineage. Most yeast strains with specific gene deletions were generated in our laboratories or by the *Saccharomyces* Genome Deletion Project (48) and were purchased from Thermo Scientific (Table 1). EN60, a strain lacking nine arrestin genes (42), referred to below as the *9Arr*Δ strain, was kindly provided by Hugh Pelham (MRC Laboratory of Molecular Biology, Cambridge, United Kingdom). Cells were grown at 30°C using a standard synthetic complete medium lacking nutrients needed for plasmid selection (49). The plasmids employed in this study are described in Table 2.

Mutagenesis. Oligonucleotide-directed mutagenesis was performed with *Pfu* polymerase, followed by DpnI digestion of the plasmid template (50). All of the mutations were confirmed by DNA sequencing. The constructs expressing Rod1-3HA and Rog3-3HA were the gift of Christopher Alvaro (UC Berkeley).

2-Deoxyglucose resistance assays. Resistance to 2DG was measured in liquid culture growth assays (7). Fresh overnight cultures were diluted in fresh medium to an A_{600} of 0.1 in the absence or presence of a range of 2DG concentrations: 0.01, 0.02, 0.05, 0.1, and 0.2 g/100 ml. Cells were grown for 18 h, and the final A_{600} was measured. Cell growth was plotted relative to growth in the absence of 2DG, defined as 100%.

Immunoblotting. Yeast whole-cell extracts were prepared using the trichloroacetic acid (TCA) extraction method (51). The Rod1 and Rog3 proteins tagged with the hemagglutinin (HA) epitope were detected with a 1:3,000 dilution of a mouse anti-HA antibody (Santa Cruz Biotechnology, Santa Cruz, CA). Green fluorescent protein (GFP)-tagged proteins were detected with a 1:1,000 dilution of a mouse anti-GFP antibody (catalog no. sc-9996; Santa Cruz Biotechnology). The secondary antibody was DyLight 680-conjugated goat anti-mouse IgG (Thermo Scientific, Waltham, MA) diluted 1:10,000. Blots were normalized by using Sec61 as the control protein, detected with an affinity-purified anti-Sec61 primary antibody at 1:1,000 (a gift of Jeffrey Brodsky, Department of Biological Sciences, University of Pittsburgh) followed by an IRDye 800CW-conjugated goat anti-rabbit secondary antibody (Li-Cor, Lincoln, NE) diluted 1:10,000. For phosphatase treatments, yeast whole-cell extracts were treated with calf intestinal alkaline phosphatase (CIP; New England BioLabs, Ipswich, MA) for 1 h at 37°C, followed by TCA precipitation. Rod1-3HA was immunoprecipitated from whole-cell extracts by using an agarose-conjugated anti-HA antibody (Santa Cruz), and ubiquitinated species were detected with a mouse antibody against ubiquitin (Ub) (catalog no. sc-8017; Santa Cruz) followed by DyLight 680-conjugated goat anti-mouse IgG (Thermo Scientific). Blots were scanned using an infrared

Downloaded from http://mcb.asm.org/ on February 22, 2015 by University of Pittsburgh HSLS

TABLE 2 Plasmids

Name	Description	Reference or source
pRS425-Rod1-3×HA	*ROD1prom-ROD1-3×HA* 2μ *LEU2*	This study
pRS425-Rog3-3×HA	*ROG3prom-ROG3-3×HA* 2μ *LEU2*	This study
pRS316-Aly1	Genomic clone of *ALY1*; CEN *URA3*	61
pRS316-Aly2	Genomic clone of *ALY2*; CEN *URA3*	61
pRS316-Rod1	Genomic clone of *ROD1* with 553 bp upstream of ATG and 250 bp downstream of the stop codon cloned into pRS316 with NotI and XmaI restriction adaptors, respectively; CEN *URA3*	This study
pRS316-Rog3	Genomic clone of *ROG3* with 520 bp upstream of ATG and 260 bp downstream of the stop codon cloned into pRS316 with NotI and XmaI restriction adaptors, respectively; CEN *URA3*	This study
pRS316-Ldb19	Genomic clone of *LBD19* with 470 bp upstream of ATG and 189 bp downstream of the stop codon cloned into pRS316 with NotI and XmaI restriction adaptors, respectively; CEN *URA3*	This study
pRS316-Art5	Genomic clone of *ART5* with 534 bp upstream of ATG and 231 bp downstream of the stop codon cloned into pRS316 with NotI and XmaI restriction adaptors, respectively; CEN *URA3*	This study
pRS316-Art10	Genomic clone of *ART10* with 523 bp upstream of ATG and 297 bp downstream of the stop codon cloned into pRS316 with NotI and XmaI restriction adaptors, respectively; CEN *URA3*	This study
pRS316-Csr2	Genomic clone of *CRS2* with 499 bp upstream of ATG and 264 bp downstream of the stop codon cloned into pRS316 with NotI and XmaI restriction adaptors, respectively; CEN *URA3*	This study
pRS316-Ecm21	Genomic clone of *ECM21* with 482 bp upstream of ATG and 212 bp downstream of the stop codon cloned into pRS316 with NotI and XmaI restriction adaptors, respectively; CEN *URA3*	This study
pRS426-Rod1	Genomic clone of *ROD1* with 553 bp upstream of ATG and 250 bp downstream of the stop codon cloned into pRS426 with NotI and XmaI restriction adaptors, respectively; 2μ *URA3*	This study
pRS426-Rod1-S447E	Genomic clone of *rod1-S447E* made by site-directed mutagenesis; 2μ *URA3*	This study
pRS426-Rod1-S447A	Genomic clone of *rod1-S447A* made by site-directed mutagenesis; 2μ *URA3*	This study
pRS426-Rod1-PPXY-less	Genomic clone of *rod1-PPXY-less*; 2μ *URA3*; the P488A, Y490A, P657A, and Y659A mutations were introduced by site-directed mutagenesis	This study
pRS426-Rod1-4KR	Genomic clone of *rod1-4KR*; 2μ *URA3*; the K235R, K245R, K264R, and K267R mutations were introduced by site-directed mutagenesis	This study
pRS426-Rog3	Genomic clone of *ROG3* with 520 bp upstream of ATG and 260 bp downstream of the stop codon cloned into pRS426 with NotI and XmaI restriction adaptors, respectively; 2μ *URA3*	This study
pRS426-Rog3-V/PPXY-less	Genomic clone of *rog3-V/PPXY-less*; 2μ *URA3*; the P461A, Y463A, P609A, Y611A, P626A, and Y628A mutations were introduced by site-directed mutagenesis	This study
pRS426-Rog3-4KR	Genomic clone of *rog3-4KR*; 2μ *URA3*; the K235R, K245R, K264R, and K267R mutations were introduced by site-directed mutagenesis	This study
pRS315-Hxt1-GFP	Genomic clone of *HXT1* with a C-terminal fusion to GFP; CEN *LEU2*	This study
pVTU100-Hxt1	*ADH1* promoter fusion to *HXT1-GFP*; 2μ *URA3*	86
YGPM20m23	Overexpression plasmid containing *HXT1* and *HXT4*; 2μ *LEU2*	28
YGPM32p17	Overexpression plasmid containing *HXT2*; 2μ *LEU2*	28
YGPM32e04	Overexpression plasmid containing *HXT3* and *HXT6*; 2μ *LEU2*	28
YGPM25j18	Overexpression plasmid containing *HXT3*; 2μ *LEU2*	28
YGPM27l21	Overexpression plasmid containing *HXT5*; 2μ *LEU2*	28
YGPM23m16	Overexpression plasmid containing *HXT7*; 2μ *LEU2*	28
YGPM25e12	Overexpression plasmid containing *HXT8*; 2μ *LEU2*	28
YGPM6d09	Overexpression plasmid containing *HXT9*; 2μ *LEU2*	28
YGPM25k04	Overexpression plasmid containing *HXT10*; 2μ *LEU2*	28
YGPM19n04	Overexpression plasmid containing *HXT11*; 2μ *LEU2*	28
YGPM2g07	Overexpression plasmid containing *HXT13*; 2μ *LEU2*	28
YGPM33e09	Overexpression plasmid containing *HXT14*; 2μ *LEU2*	28
YGPM33c02	Overexpression plasmid containing *RGT2*; 2μ *LEU2*	28
YGPM12p11	Overexpression plasmid containing *SNF3*; 2μ *LEU2*	28
YGPM17p07	Overexpression plasmid containing *GAL2*; 2μ *LEU2*	28
pHXT1-425	*HXT1* gene from YGPM20m23 cloned into pRS425; 2μ *LEU2*	This study
pHXT4-425	*HXT4* gene from YGPM20m23 cloned into pRS425; 2μ *LEU2*	This study
pHXT6-425	*HXT6* gene from YGPM32e04 cloned into pRS425; 2μ *LEU2*	This study
YGPM10o10	Overexpression plasmid containing *DOG1* and *DOG2* genes; 2μ *LEU2*	28
pHXT1-lacZ	*HXT1* promoter driving expression of the *lacZ* gene; 2μ *URA3*	29
pHXT3-lacZ	*HXT3* promoter driving expression of the *lacZ* gene; 2μ *URA3*	29

scanner (Odyssey; Li-Cor). The integrated intensities of bands were quantified by using scanning software supplied by the manufacturer (Li-Cor).

LacZ assays. To assess the levels of expression of reporter genes whose promoters were fused to *Escherichia coli lacZ*, yeast cells were grown to mid-exponential phase in a high-glucose medium either alone or with 0.05% 2DG and were lysed by vortex mixing with glass beads. Samples of the resulting extracts were assayed for β-galactosidase activity in triplicate (52).

Downloaded from http://mcb.asm.org/ on February 22, 2015 by University of Pittsburgh HSLS

Fluorescence microscopy. The GFP-tagged glucose transporters Hxt1 and Hxt3 were imaged using an inverted Ti Eclipse swept-field confocal microscope (Nikon, Chiyoda, Tokyo, Japan; Prairie Instruments, Middleton, WI) fitted with an Apo 100× objective (numerical aperture, 1.49). Images were captured using an electron-multiplying charge-coupled device camera (iXon3; Andor, Belfast, United Kingdom) and NIS-Elements software (Nikon). The day before imaging, cells were grown overnight to saturation in selective, synthetic complete medium at 30°C. The cells were diluted the next morning into fresh medium and were regrown to mid-exponential phase (A_{600}, 0.5); then either 0.2% glucose or 0.2% 2DG was added. The cells were incubated further at 30°C for 0 to 120 min, as indicated in the figures, prior to imaging. For experiments where cells were treated with latrunculin A (Lat A), cultures were grown to early-exponential phase (A_{600}, 0.3), treated for 90 min either with an equivalent volume of the solvent (dimethyl sulfoxide [DMSO]) alone or with 200 μM (final concentration) Lat A (Life Technologies, Carlsbad, CA) from a stock dissolved in DMSO, and then further incubated with 0.2% 2DG for 90 min at 30°C. Prior to imaging, cells in the Lat A experiments were stained with FM 4-64 (see below) to assess the degree of inhibition of endocytosis. Cells were plated onto glass-bottom dishes (MatTek, Ashland, MA) coated with concanavalin A (Sigma, St. Louis, MO) and were allowed to settle for 5 min prior to imaging. Prior to imaging, cells in the *RSP5* and *rsp5-1* backgrounds were grown at a permissive temperature (23°C) from an A_{600} of 0.2 for 4 h and were shifted to a restrictive temperature (37°C) for 30 min prior to 2DG addition. All images from an experiment were captured with identical imaging parameters and were equivalently adjusted using Adobe Photoshop software. For most figures, an unsharp mask filter was applied to the images with a threshold of 5 levels and a pixel radius of 3.

Vacuolar staining. To visualize vacuoles, cells were incubated with 250 μM CellTracker Blue CMAC (7-amino-4-chloromethylcoumarin) dye (Life Technologies, Carlsbad, CA) for 15 to 30 min. Cells were then pelleted, washed, and resuspended prior to imaging. As a control in the Lat A experiments, cells were costained with FM 4-64 (53) by first incubating the cells in a medium with 1.6 μM FM 4-64 for 20 min, then pelleting them, resuspending them in fresh medium without FM 4-64 but containing DMSO, Lat A, and/or 2DG, and finally incubating them for a further 15 min (to allow time for dye internalization) before imaging.

Fluorescence quantification. The fluorescence intensities of Hxt1-GFP and Hxt3-GFP were quantified using ImageJ software (NIH, Bethesda, MD). For the quantification of fluorescence at the cell surface, the plasma membrane (PM) in each of at least 150 cells was manually outlined using ImageJ software, mean pixel intensity measured, and mean background pixel intensity subtracted (43). The distribution of mean pixel intensities (in arbitrary units) and the distribution of pixel intensities for each cell population are presented as box-and-whisker plots. Nonparametric, two-tailed Mann-Whitney U tests were performed using Prism software (GraphPad, La Jolla, CA), and statistically significant differences are indicated in figures by using asterisks as described in the next section. For the quantification of fluorescence in the vacuole, vacuole profiles revealed by CMAC dye were used to generate a mask in ImageJ, which was then overlaid on the Hxt1-GFP or Hxt3-GFP image; the GFP signal congruent with the vacuole was measured; and mean background fluorescence intensity was subtracted. Each vacuole identified in a given field was then paired with a corresponding measurement of PM fluorescence, performed as described above. Prism software and nonparametric, two-tailed Mann-Whitney U tests were used to assess the significance of changes in the vacuole fluorescence distribution and PM/vacuolar fluorescence ratios. When three or more comparisons were made across groups (see, e.g., Fig. 4I and J), rather than the Mann-Whitney U test, we used one-way analysis of variance (ANOVA) with the nonparametric Kruskal-Wallis test and Dunn's multiple-comparison *post hoc* analyses using Prism software. In the absence of a vacuolar costain, the ratio of PM fluorescence to intracellular fluorescence was determined by manually contouring PMs and then pairing each with a measure of total intracellular fluorescence, assigned manually using ImageJ software. Since the vast majority of intracellular fluorescence arises from the vacuole in these cells, this PM/intracellular fluorescence ratio is representative of the approximate PM/vacuole ratio.

Statistical significance. For all bar plots, each mean value represents the average for a minimum of three independent measurements, and the error bars represent 1 standard error. Statistical significance was determined using the Student *t* test for unpaired variables with equal variance.

RESULTS

***HXT1* and *HXT3* are dosage suppressors of the 2DG hypersensitivity of *snf1*Δ cells.** Yeast cell growth is inhibited by low concentrations of 2DG. We and others have shown that sensitivity to 2DG differs depending on the carbon source (7, 12). We found that cells growing on glucose were the most resistant and those growing on a nonfermentable carbon source (glycerol/ethanol) were the most sensitive (7). Strikingly, we also found that cells lacking Snf1 exhibit a 2DG-hypersensitive phenotype, even when growing on glucose. To gain insight into the 2DG-hypersensitive phenotype of *snf1*Δ cells and the mechanism of action of 2DG, we transformed *snf1*Δ cells with a systematically constructed, comprehensive genomic DNA library in a multicopy vector (28) and selected for clones that conferred a growth advantage on the *snf1*Δ cells in glucose medium containing 0.01% 2DG. As expected, we recovered the clone overexpressing Snf1 (not shown). In addition, we isolated multiple clones that carried hexose transporter genes. Strong suppression of the 2DG hypersensitivity of *snf1*Δ cells was observed with three plasmids, one carrying *HXT1* and *HXT4*, one carrying *HXT3* and *HXT6*, and one carrying *HXT3* alone. Subclones generated in the high-copy-number plasmid pRS425 demonstrated that the *HXT1* and *HXT3* genes, not the *HXT4* or *HXT6* gene, were responsible for the suppression (not shown). The inability of *HXT4* to suppress the 2DG-hypersensitive phenotype of *snf1*Δ cells was not due to lack of expression, since Hxt4-GFP overexpressed from a high-copy-number plasmid was detected at the cell surface (not shown).

Given these findings, we tested directly all library clones that contained a hexose transporter gene(s) for their abilities to ameliorate the 2DG hypersensitivity of *snf1*Δ cells. In agreement with the results of our screen, only clones containing *HXT1* or *HXT3* were strong suppressors (Fig. 1). Overexpression of *HXT2* weakly suppressed the 2DG-hypersensitive phenotype, but this suppression was not strong enough to have been detected in our original screen.

Earlier selections for dosage suppressors that confer 2DG resistance were conducted in *SNF1*$^+$ cells and identified the *DOG1* and *DOG2* genes, linked paralogs encoding enzymes with 2DG-6P phosphatase activity (54). Dog1 and Dog2 confer 2DG resistance on cells growing on alternative carbon sources by preventing the accumulation of 2DG-6P, presumably alleviating the inhibition of glycolysis. Hence, we compared the effect of *DOG1* and *DOG2* overexpression with that of *HXT1* on the 2DG resistance of wild-type cells in either glucose- or sucrose-containing medium and on that of *snf1*Δ cells in glucose medium (cells lacking Snf1 are unable to grow on sucrose). In glucose-grown *snf1*Δ cells, *HXT1* overexpression conferred a strong growth advantage over a wide range of 2DG concentrations, whereas *DOG1* and *DOG2* overexpression had no discernible effect (Fig. 2A). When the same comparison was conducted in wild-type (*SNF1*$^+$) cells, *DOG1* and *DOG2* overexpression conferred significant 2DG resistance, whereas *HXT1* overexpression had a more modest effect (Fig. 2B). Wild-

Downloaded from http://mcb.asm.org/ on February 22, 2015 by University of Pittsburgh HSLS

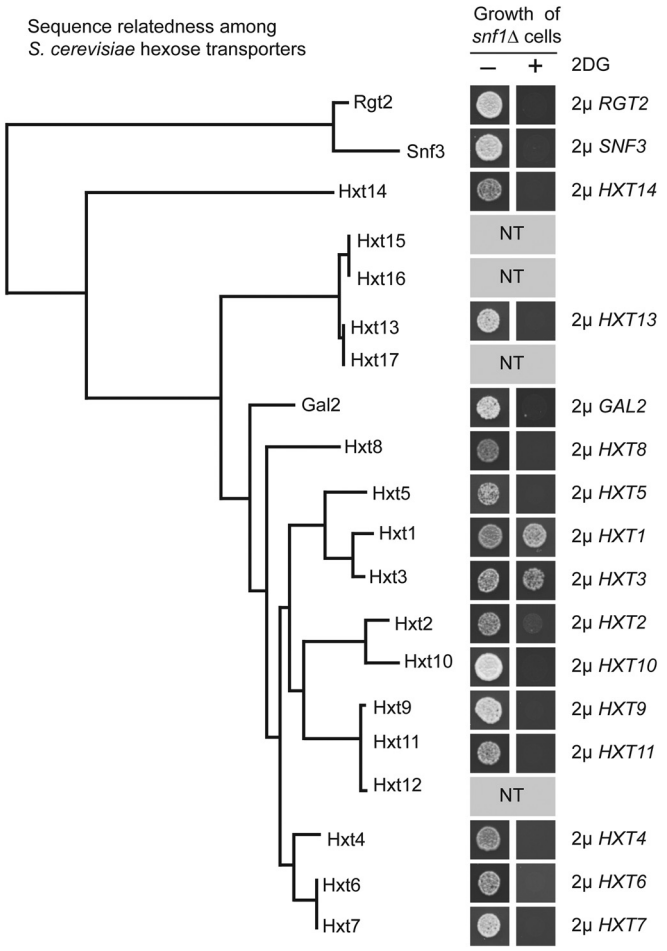

FIG 1 Hexose transporters of *S. cerevisiae* and suppression of 2DG hypersensitivity in *snf1*Δ cells. (Left) A dendrogram of the 20 yeast hexose transporters based on their amino acid sequence relatedness was generated using ClustalW (83). (Right) Growth was assayed in *snf1*Δ cells with overexpressed *HXT* genes in medium with (+) or without (−) 2DG. NT, not tested, because the gene was not in the overexpression library (28).

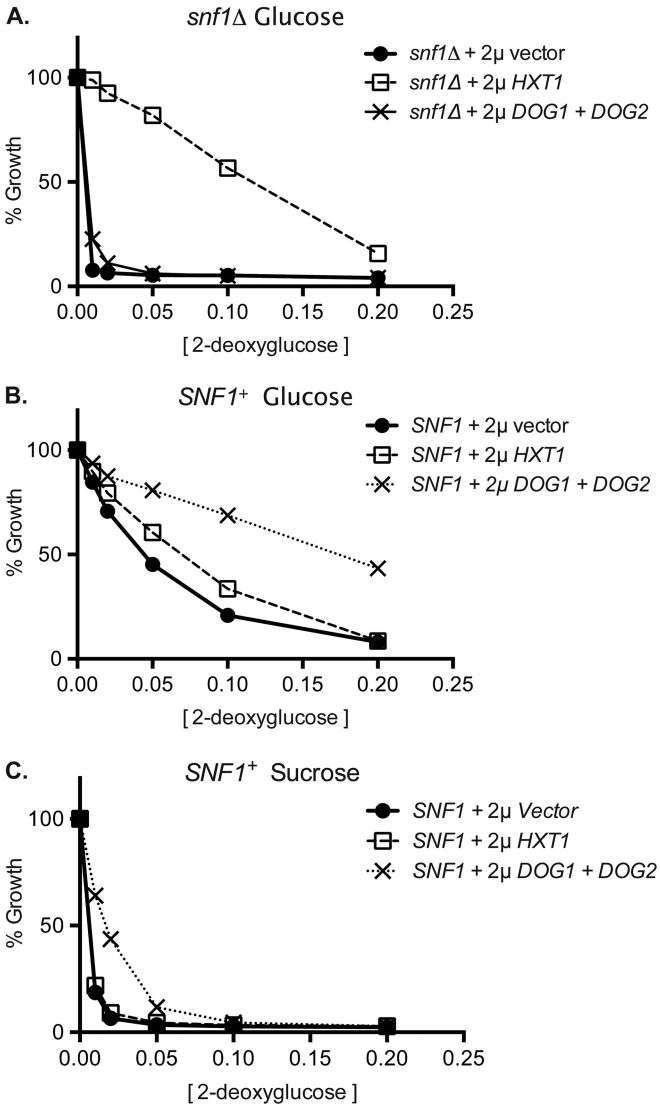

FIG 2 Effect of overexpression of *HXT1* or *DOG1* plus *DOG2* on 2DG resistance. Cells were transformed with high-copy-number plasmids expressing either *HXT1*, *DOG1* and *DOG2*, or an empty vector. 2DG resistance was assayed in *snf1*Δ cells growing on glucose (A) or in wild-type cells growing on glucose (B) or on sucrose (C).

type cells grown on sucrose are more sensitive to 2DG than cells grown on glucose (7). On this carbon source, *DOG1* and *DOG2* overexpression conferred a readily detectable growth advantage in the presence of 2DG (Fig. 2C), whereas *HXT1* did not, presumably because *HXT1* is poorly expressed in the absence of glucose (29). These results suggested that *snf1*Δ cells have defects in hexose transporter expression, localization, and/or function that cannot be ameliorated by the action of Dog1 and Dog2.

2DG reduces Hxt1 and Hxt3 expression and protein levels and stimulates trafficking to the vacuole. To assess *HXT1* and *HXT3* transcription in response to 2DG, we employed *HXT* promoter-*lacZ* fusions, which have been used to evaluate the carbon source-dependent expression patterns of hexose transporters (29). In wild-type cells, *HXT1* and *HXT3* expression was significantly decreased upon 2DG addition (Fig. 3A and B). In *snf1*Δ cells, basal *HXT1* and *HXT3* expression was lower than in wild-type cells and was further dampened upon 2DG addition. These findings demonstrate that Snf1 function is required for optimal *HXT1* and *HXT3* expression on glucose and also that one previously uncharacterized effect of 2DG is to impede the expression of these transporter genes. Loss of Reg1 greatly reduced *HXT1* and *HXT3* expression in either the absence or the presence of 2DG (Fig. 3A and B). Reg1 is the regulatory subunit of Glc7, the type 1 protein phosphatase (PP1) responsible for the dephosphorylation and inactivation of Snf1 (55–57). In *reg1*Δ cells, Snf1 is constitutively phosphorylated and active (58, 59), and therefore, one might have expected *reg1*Δ cells to display the opposite phenotype from *snf1*Δ cells. Since this is not the case, our results suggest that some other Reg1-dependent PP1 action is required for the transcription of the *HXT1* and *HXT3* genes. In any event, the effects observed on *HXT1* and *HXT3* at the transcriptional level were reflected in the steady-state levels of the proteins encoded, with (i) reduced Hxt1 and Hxt3 levels in wild-type cells after 2DG addition, (ii) lower Hxt1 and Hxt3 levels in *snf1*Δ cells than in wild-type cells and further reduction upon 2DG addition, and (iii) al-

Downloaded from http://mcb.asm.org/ on February 22, 2015 by University of Pittsburgh HSLS

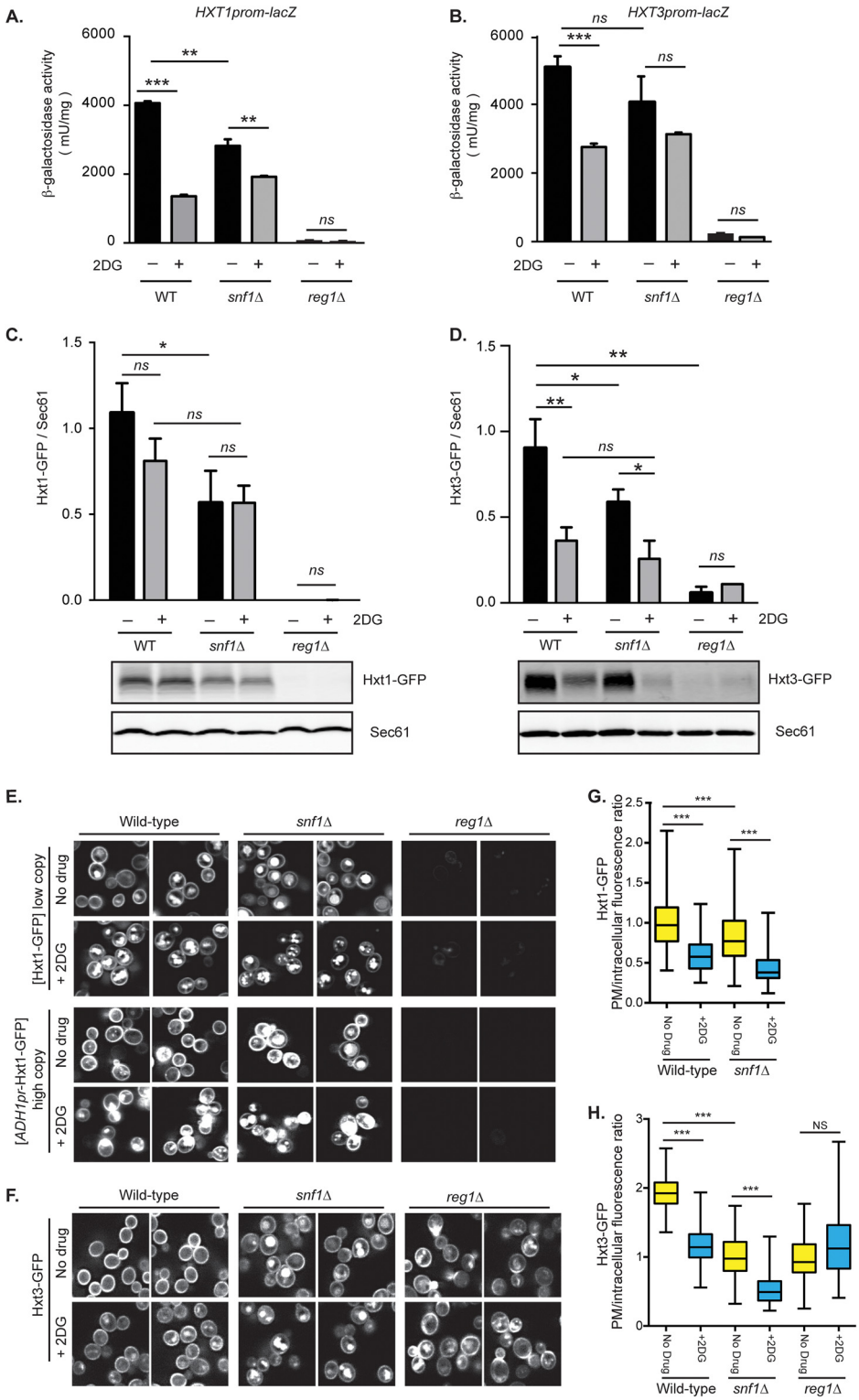

FIG 3 Effects of 2DG on *HXT1* and *HXT3*. (A and B) Extracts were prepared from wild-type (WT), *snf1*Δ, and *reg1*Δ cells containing either p*HXT1prom-lacZ* or p*HXT3prom-lacZ* as indicated. Mean β-galactosidase activities ± standard errors were plotted for cells grown with or without 0.05% 2DG. (C and D) Protein extracts were prepared from wild-type, *snf1*Δ, and *reg1*Δ cells with a chromosomal *HXT1-GFP* or *HXT3-GFP* gene, with or without 2DG, for 2 h. Proteins were analyzed by immunoblotting, and the mean Hxt-GFP/Sec61 ratios ± standard errors from triplicate samples were plotted. (E and F) Wild-type, *snf1*Δ, and *reg1*Δ cells containing either Hxt1-GFP, expressed from the endogenous *HXT1* promoter or from the *ADH1* promoter (E), or a chromosomal *HXT3-GFP* gene (F) were examined after 2 h of treatment with 0.2% glucose (no drug) or 0.2% 2DG. (G and H) The PM and intracellular GFP fluorescence intensities from the cells depicted in panels E and F, respectively, were quantified, and the distributions of the PM/intracellular GFP fluorescence ratios were plotted (*n*, >110 cells). The horizontal midline represents the median; the box is bounded by the upper and lower quartiles; and the whiskers denote the maximal and minimal fluorescence intensities. *, $P < 0.05$; **, $P < 0.01$; ***, $P < 0.001$; NS or ns, $P > 0.05$.

Downloaded from http://mcb.asm.org/ on February 22, 2015 by University of Pittsburgh HSLS

most no detectable Hxt1 and reduced Hxt3 levels in *reg1*Δ cells (Fig. 3C and D).

We next examined the localizations of Hxt1-GFP and Hxt3-GFP. In wild-type cells in a high-glucose medium, both proteins displayed a prominent signal at the PM with variable fluorescence in the vacuole, whereas by 2 h after the addition of 2DG, the PM fluorescence for Hxt1 and Hxt3 was substantially reduced, while vacuolar fluorescence was dramatically increased (Fig. 3E and F). These observations are further supported by quantification of the PM/intracellular fluorescence ratio (Fig. 3G and H), which was significantly decreased upon 2DG addition and was lower in *snf1*Δ cells than in wild-type cells under either the basal condition or 2DG treatment. Thus, exposure to 2DG appears to stimulate the internalization of Hxt1 and Hxt3. In the absence of Snf1, the 2DG-stimulated internalization of Hxt1 and Hxt3 was even more pronounced (Fig. 3E to H), suggesting that Snf1 inhibits the endocytosis and/or vacuolar trafficking of these transporters. In agreement with the drastically reduced *HXT1* expression observed in *reg1*Δ cells (Fig. 3A and C), it was difficult to detect this transporter (Fig. 3E). Additionally, Hxt3-GFP fluorescence is reduced in *reg1*Δ cells, with considerable vacuolar fluorescence even before 2DG addition (Fig. 3F). These changes in Hxt1 and Hxt3 protein levels and localization are not strictly due to alterations in gene expression, however, since Hxt1-GFP expressed from the strong constitutive *ADH1* promoter exhibited similar protein abundance and localization changes in response to 2DG (Fig. 3E, bottom). These data indicate that Snf1, Reg1, and 2DG control Hxt transcription, abundance, and localization.

We followed the localization of Hxt1-GFP and Hxt3-GFP in response to 2DG treatment during a more detailed time course and used a dye (CMAC blue) that marks the vacuole to confirm that the observed intracellular fluorescence was vacuole associated. We found that: (i) in glucose-grown cells in the absence of 2DG, the majority of Hxt1 (Fig. 4A) and Hxt3 (Fig. 4B) resided at the cell surface; (ii) within 20 min after exposure to 0.2% 2DG, dim vacuolar fluorescence was observed; (iii) during the course of incubation, vacuolar fluorescence increased continuously and in an increasing proportion of the cells; and (iv) conversely, PM fluorescence was progressively diminished over the course of the incubation (Fig. 4C and D), with a concomitant increase in vacuolar fluorescence (Fig. 4E and F).

To confirm that the increase in vacuolar fluorescence caused by 2DG treatment was due to endocytosis, we preincubated cells with Lat A and then treated them with 2DG. Lat A prevents actin polymerization and blocks endocytosis while leaving intracellular vesicle-mediated sorting intact (60). As a control to determine the effectiveness of the Lat A block to endocytosis, cells in the same assay were costained with FM 4-64, a lipophilic dye that binds the PM but then is rapidly concentrated in the vacuolar membrane when endocytosis is functional (53); as expected, FM 4-64 remained predominantly at the surfaces of Lat A-treated cells, whereas in vehicle (DMSO)-treated cells, FM 4-64 was confined to the limiting membrane of the vacuole (data not shown). When cells expressing Hxt1-GFP or Hxt3-GFP were pretreated with Lat A, they no longer exhibited reduced PM fluorescence in response to 2DG (Fig. 4G, H, I, and J), demonstrating that 2DG stimulates the endocytosis of Hxt1 and Hxt3. However, even in Lat A-treated cells, vacuolar fluorescence increased after 2DG addition (Fig. 4G and H), suggesting that 2DG may also divert Hxt1-GFP and Hxt3-GFP from the Golgi compartment or another intracellular compartment to the vacuole.

Endocytosis of Hxt1 and Hxt3 stimulated by 2DG requires the α-arrestins Rod1 and Rog3. The internalization and trafficking to the vacuole of many nutrient transporters are regulated by α-arrestins (38, 40, 42, 43, 45, 47, 61). These proteins facilitate protein sorting by serving as adaptors that recruit the ubiquitin ligase Rsp5 to select cargos. We suspected that α-arrestins might be involved in the 2DG-stimulated internalization of Hxt1 and Hxt3 for three reasons. First, Rod1, one of the 13 known yeast α-arrestins, has been shown to regulate the glucose-stimulated endocytosis of hexose transporter Hxt6 (42). Second, this α-arrestin is phosphorylated by Snf1 (62), which negatively regulates Rod1-mediated endocytosis of the lactate permease Jen1 (38). Finally, a mammalian α-arrestin involved in downregulating the glucose transporter GLUT1 is also negatively regulated by AMPK (27). We sought to determine if the 2DG-induced trafficking of Hxt1 and Hxt3 was regulated by α-arrestins. Indeed, in a mutant strain (*9Arr*Δ) lacking 9 of the 13 α-arrestins (42), 2DG no longer triggered the internalization of Hxt1-GFP or Hxt3-GFP (Fig. 5A and B), and the reductions in the steady-state levels of Hxt1 and Hxt3 observed in wild-type cells treated with 2DG were prevented (Fig. 5C and D).

To determine whether any of the 9 α-arrestins missing in *9Arr*Δ cells were sufficient for 2DG-stimulated Hxt1-GFP and/or Hxt3-GFP endocytosis, the mutant was complemented with plasmids expressing each of these nine genes. For Hxt1-GFP, only *ROD1* expression restored 2DG-stimulated internalization and vacuolar trafficking (Fig. 5E), whereas for Hxt3-GFP, either *ROD1* or its paralog *ROG3* could do so potently, and *CSR2* could do so only very weakly (Fig. 5F). Indeed, Rod1 appears to be responsible for the 2DG-stimulated endocytosis of Hxt1-GFP, because Hxt1-GFP internalization after 2DG addition was ablated in *rod1*Δ cells but was not markedly diminished in *rog3*Δ cells (Fig. 6A). In contrast, Hxt3-GFP internalization in response to 2DG was significantly reduced in *rod1*Δ cells and not at all in *rog3*Δ cells but was totally prevented in a *rod1*Δ *rog3*Δ double mutant (Fig. 6B). Interestingly, in the absence of Rog3, the removal of Hxt3-GFP from the cell surface and its accumulation in the vacuole appeared to be greatly enhanced (Fig. 6B), suggesting that the endocytosis of this transporter mediated by Rod1 (or perhaps another α-arrestin) is increased in the absence of Rog3. These data demonstrate new and distinct roles for Rod1 and Rog3 in regulating the trafficking of hexose transporters.

Snf1 negatively regulates Rod1- and Rog3-dependent endocytosis of Hxt1 and Hxt3. In cells lacking Snf1, basal and 2DG-induced vacuolar accumulation of Hxt1-GFP was elevated, but these effects were almost completely eliminated in *snf1*Δ cells that also lacked Rod1 and Rog3 (Fig. 6C). This epistasis suggests that with respect to hexose transporter trafficking, a primary function of Snf1 is to negatively regulate Rod1 and Rog3. Growth experiments supported this conclusion; the 2DG hypersensitivity of *snf1*Δ cells was substantially rescued by the removal of Rod1 alone (Fig. 6D), and growth was further enhanced by the removal of both Rod1 and Rog3 (Fig. 6E) but not by the removal of Rog3 alone (Fig. 6D). Even the growth of wild-type cells in the presence of 2DG was increased by removal of both Rod1 and Rog3 (Fig. 6E). These findings strongly suggest that the inhibition of cell growth on a glucose medium after challenge with 2DG is due primarily to the α-arrestin-mediated downregulation of Hxt1 and

Downloaded from http://mcb.asm.org/ on February 22, 2015 by University of Pittsburgh HSLS

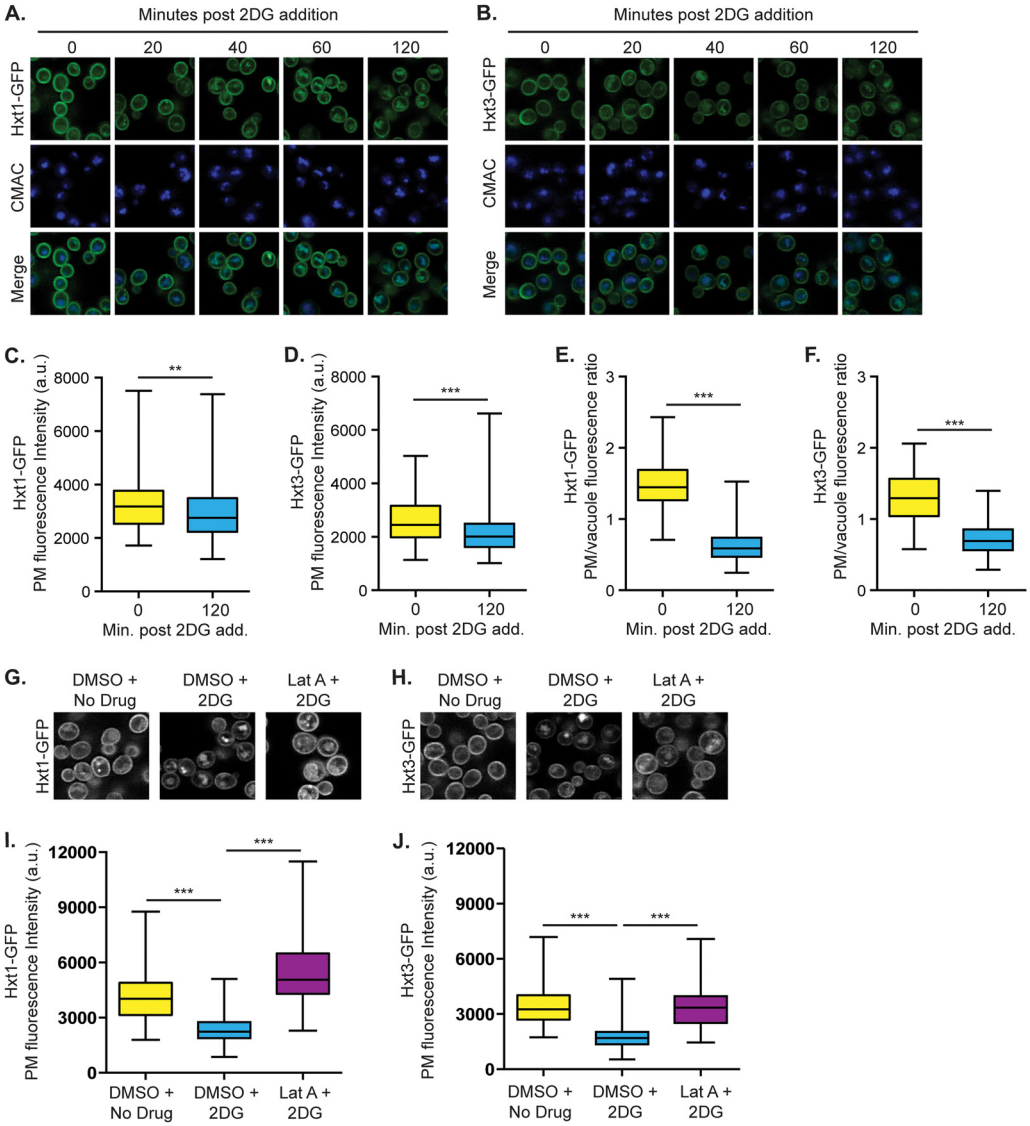

FIG 4 2DG promotes the vacuolar localization of Hxt1 and Hxt3. (A and B) Wild-type cells with integrated Hxt1-GFP or Hxt3-GFP were stained with CMAC blue and were treated with 2DG. Images were captured at the times indicated after 2DG addition. (C and D) The mean PM fluorescence intensities of Hxt1-GFP or Hxt3-GFP before and 120 min after 0.2% 2DG addition were measured, and the distributions of these intensities were plotted. (E and F) The ratio of cell surface fluorescence to vacuolar fluorescence for Hxt1-GFP or Hxt3-GFP was determined (n, >150 cells), and the distributions of these ratios were plotted. (G and H) Wild-type cells with integrated Hxt1-GFP or Hxt3-GFP were imaged after treatment with either 200 μM latrunculin A or the vehicle control DMSO for 2 h, followed by incubation with 0.2% 2DG for 90 min. (I and J) The PM intensities of Hxt1-GFP or Hxt3-GFP were measured (n, >110 cells), and the distributions were plotted. a.u., arbitrary units. For the box plots in panels C, D, E, F, I, and J, the horizontal midline in each box represents the median, the box is bounded by the upper and lower quartiles, and the whiskers denote the maximal and minimal fluorescence intensities. **, $P < 0.01$; ***, $P < 0.001$.

Hxt3. It has been reported that Snf1 phosphorylates Ser447 in Rod1 (62). To determine whether modification at Ser447 alone is sufficient to explain how the action of Snf1 impedes Rod1-mediated internalization of Hxt1 and Hxt3, we generated and tested both a *rod1*(S447A) and a *rod1*(S447E) allele. We found that both of these mutants supported basal and 2DG-stimulated Hxt1-GFP and Hxt3-GFP endocytosis comparably to wild-type Rod1 (Fig. 6F) and also restored sensitivity to 2DG equivalently to wild-type Rod1 (Fig. 6G). Hence, Ser447 is not an important site, or not a sufficient site, for the Snf1-dependent regulation of Rod1. Indeed, more-recent phosphoproteomic studies have identified 31 phosphorylation sites on Rod1 by mass spectroscopy (63–66). Whether any of these sites are phosphorylated by Snf1 and regulate Rod1 function will be important to determine in subsequent studies.

For Rod1-mediated internalization of another PM client, the G protein-coupled receptor (GPCR) Ste2, Rod1 must be dephosphorylated by the yeast protein phosphatase 2B calcineurin (67). Calcineurin is a Ca^{2+}/calmodulin-stimulated enzyme with two alternative catalytic subunits, Cna1 and Cna2, and an essential regulatory subunit, Cnb1 (68). However, we observed 2DG-stimulated Hxt1-GFP and Hxt3-GFP endocytosis even in *cnb1*Δ cells (data not shown); hence, calcineurin-dependent dephosphorylation of Rod1 is not required for the internalization of these transporters. Therefore, the phosphoregulation of α-arrestins

Downloaded from http://mcb.asm.org/ on February 22, 2015 by University of Pittsburgh HSLS

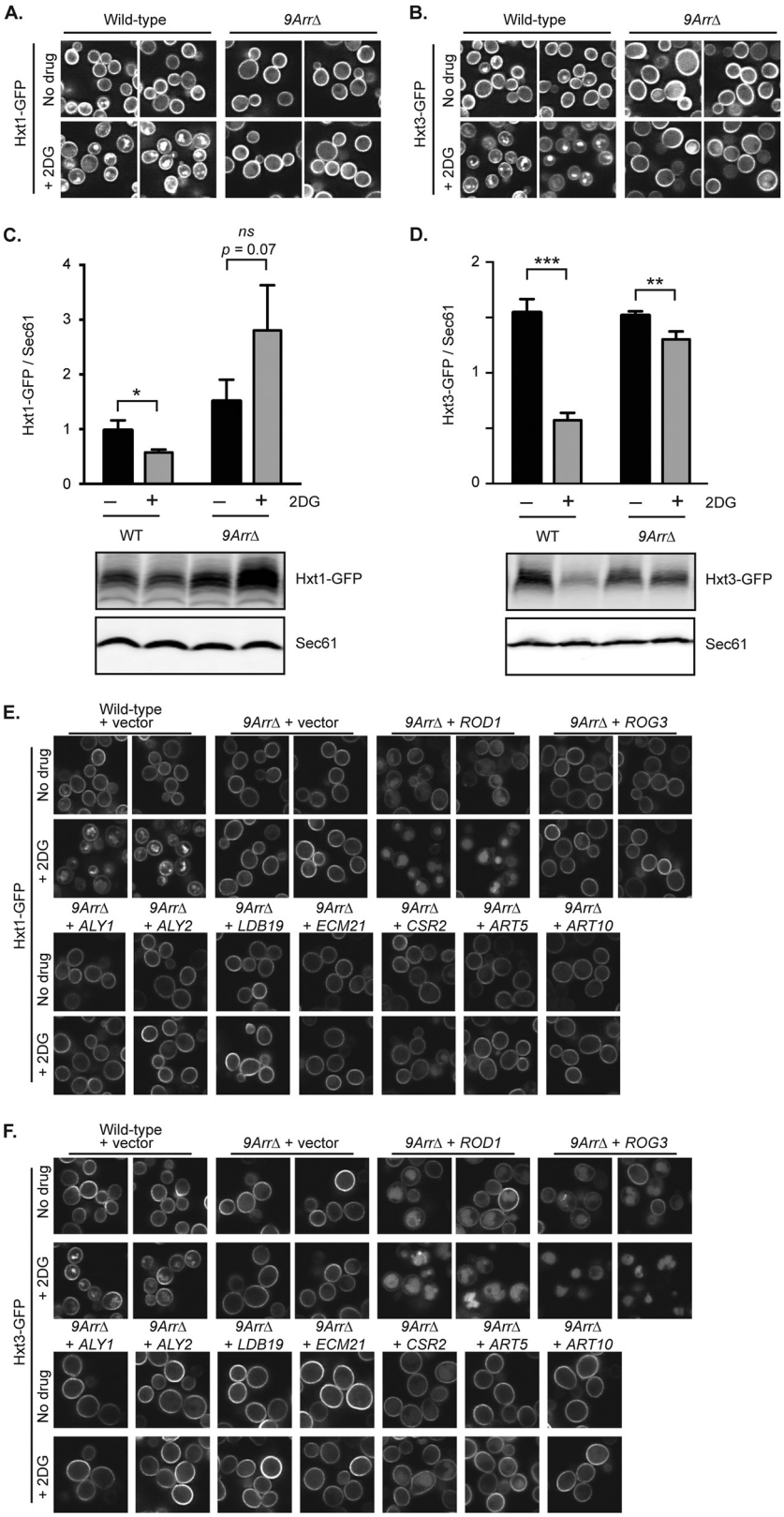

FIG 5 Hxt1 and Hxt3 vacuolar trafficking is regulated by α-arrestins. (A and B) Wild-type cells or cells lacking nine α-arrestin genes (*9Arr*Δ) containing integrated Hxt1-GFP or Hxt3-GFP were examined before or 2 h after 0.2% 2DG addition. (C and D) Protein extracts were prepared in triplicate from cells treated as for the experiments for which results are shown in panels A and B. Extracts were assessed by immunoblotting with anti-GFP and anti-Sec61 antibodies. The mean ratios of Hxt1-GFP or Hxt3-GFP to Sec61 ± standard errors were plotted. (E and F) Wild-type or *9Arr*Δ cells with integrated Hxt1-GFP (E) or Hxt3-GFP (F) and containing pRS316 (+ vector) or expressing the indicated α-arrestin were imaged either before (no drug) or after a 2-h treatment with 0.2% 2DG. *, $P < 0.05$; **, $P < 0.01$; ***, $P < 0.001$; ns, $P > 0.05$.

Downloaded from http://mcb.asm.org/ on February 22, 2015 by University of Pittsburgh HSLS

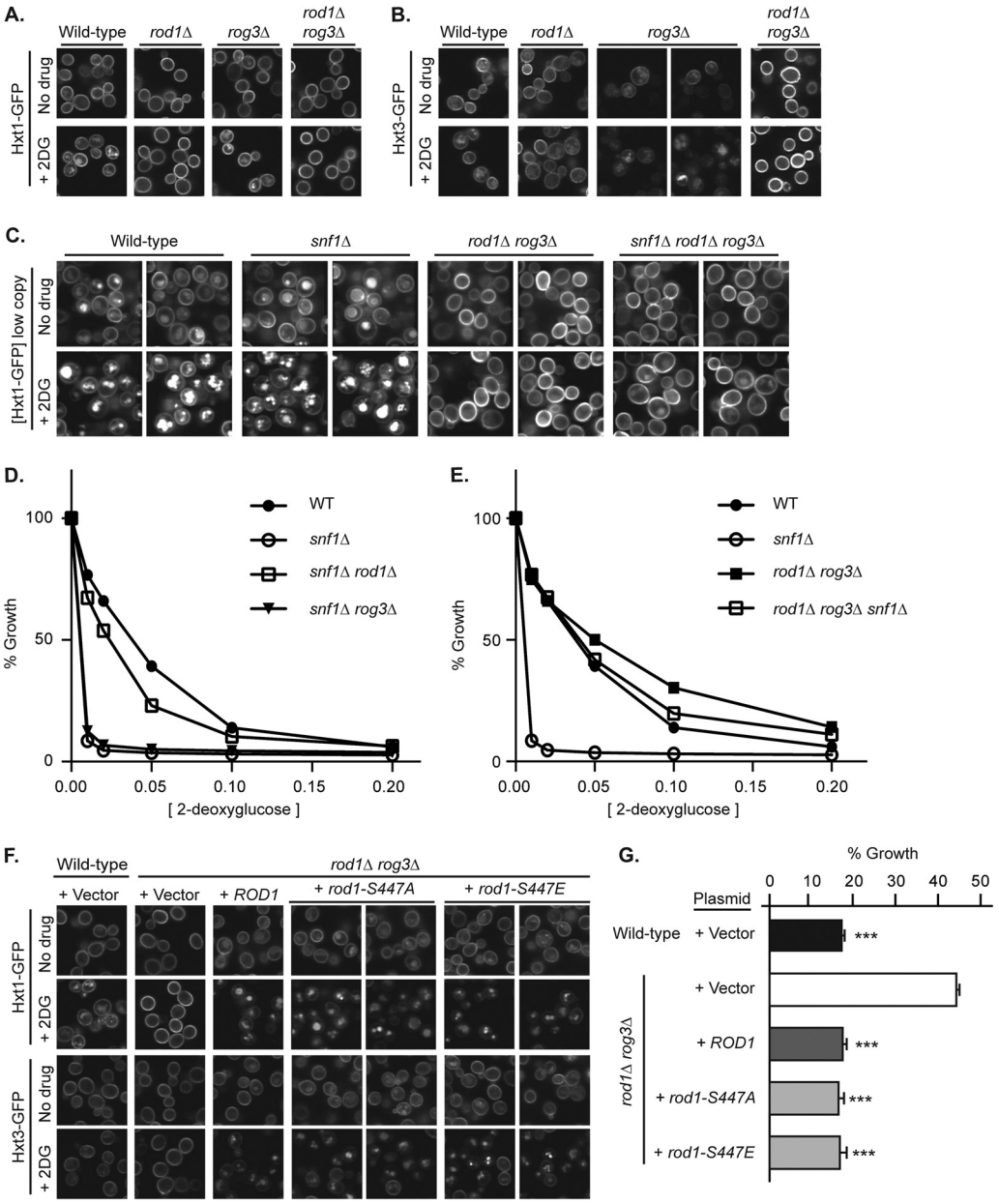

FIG 6 Deletion of *ROD1* and *ROG3* prevents the trafficking of hexose transporters to the vacuole and suppresses the 2DG hypersensitivity of *snf1*Δ cells. (A to C) Cells of the indicated genotypes containing integrated Hxt1-GFP (A), Hxt3-GFP (B), or pRS315-Hxt1-GFP (C) were imaged either before (no drug) or after a 2-h treatment with 0.2% 2DG. (D and E) Cells of the indicated genotypes were assayed for 2DG sensitivity. (F) Wild-type or *rod1*Δ *rog3*Δ cells containing integrated Hxt1-GFP or Hxt3-GFP were transformed with the indicated plasmids and were imaged either before (no drug) or after a 2-h treatment with 0.2% 2DG. (G) The cells imaged in panel F were assayed for sensitivity to 0.1% 2DG. Mean values from triplicate samples ± standard errors were plotted, and statistical significance in comparison to the value for *rod1*Δ *rog3*Δ cells transformed with vector was evaluated. ***, $P < 0.001$.

is complex, with multiple kinases and phosphatases controlling α-arrestin function.

Rod1 and Rog3 must recruit Rsp5 to downregulate Hxt1 and Hxt3. The α-arrestins contain PPXY motifs (and variants thereof, such as LPXY or VPXY), which bind the WW domains in the ubiquitin ligase Rsp5 (35, 69). This interaction recruits Rsp5 to specific cargos (37, 40, 42). In turn, Rsp5-mediated ubiquitination of nutrient transporters at the cell surface is a prelude to their endocytosis (35, 70–73). It has been reported recently that Rsp5 is required for Hxt1 and Hxt3 turnover in response to nutrient starvation (32, 33). Hxt1 and Hxt3 do not possess any PPXY or related motifs, as would be expected if the α-arrestins Rod1 and Rog3 served to deliver Rsp5 to these clients. Because mutation of the two PPXY sites in Rod1 or of two PPXY sites plus one VPXY site in Rog3 (Fig. 7A) abrogates their Rsp5 binding (38, 67), we used our growth and fluorescence microscopy assays to assess the abilities of these mutants to support 2DG-stimulated internalization of Hxt1 and Hxt3. Unlike wild-type *ROD1* and *ROG3*, *rod1-PPXY-less* and *rog3-V/PPXY-less* were unable to confer 2DG sensitivity (Fig. 7B) and failed to promote the internalization of either Hxt1-

Downloaded from http://mcb.asm.org/ on February 22, 2015 by University of Pittsburgh HSLS

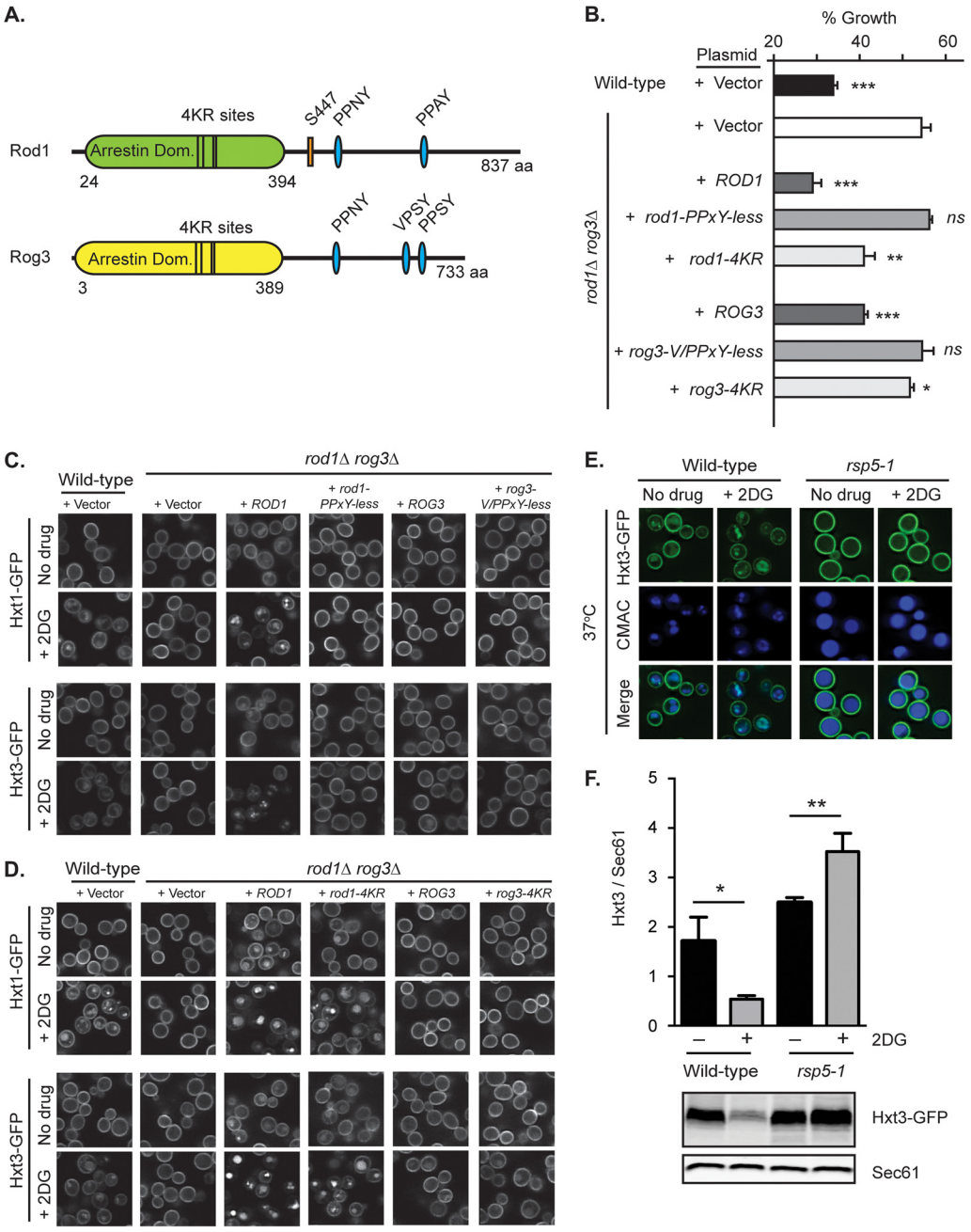

FIG 7 Rsp5 is required for the induction of vacuolar trafficking. (A) Schematic diagrams of Rod1 and Rog3. Numbers indicate amino acids. The arrestin-fold domains (Arrestin Dom.) were defined by Phyre2 structural predictions (84). The positions of the Rsp5 binding sites (VPXY and PPXY motifs), the putative Snf1-dependent phosphorylation site at S447, and the 4 conserved lysine residues that are changed to arginine (4KR sites) in order to block ubiquitination (38, 67) are indicated. (B) Wild-type or *rod1*Δ *rog3*Δ cells were transformed with the indicated plasmids and were assayed for sensitivity to 0.1% 2DG. Mean values from triplicate samples ± standard errors were plotted. (C and D) Wild-type or *rod1*Δ *rog3*Δ cells containing integrated Hxt1-GFP or Hxt3-GFP and transformed with the indicated plasmids were imaged before (no drug) or after a 2-h treatment with 0.2% 2DG. (E) Wild-type or *rsp5-1* cells containing integrated Hxt3-GFP were imaged before (no drug) or after a 2-h treatment with 0.2% 2DG at 37°C. (F) Protein extracts were prepared in triplicate from cells treated as in the experiment for which results are shown in panel E. The extracts were assessed by immunoblotting with anti-GFP and anti-Sec61 antibodies. The mean ratios of Hxt3-GFP to Sec61 ± standard errors were plotted. *, $P < 0.05$; **, $P < 0.01$; ***, $P < 0.001$; ns, $P > 0.05$.

GFP or Hxt3-GFP upon 2DG addition (Fig. 7C). Similarly, in cells where the hypomorphic *rsp5-1* allele is present, 2DG fails to induce the endocytosis of Hxt1 (data not shown) or Hxt3 (Fig. 7E), and the Hxt3-GFP protein is stabilized (Fig. 7F) when cells are incubated at a restrictive temperature. Together, these data demonstrate that Rsp5 is required for the 2DG-stimulated and Rod1- and Rog3-mediated endocytosis of Hxt1 and Hxt3.

The formation of cargo–α-arrestin–Rsp5 ternary complexes permits not only the ubiquitination of the cargo but also the ubiquitination of the α-arrestin. For some, but not all, α-arrestin–

Downloaded from http://mcb.asm.org/ on February 22, 2015 by University of Pittsburgh HSLS

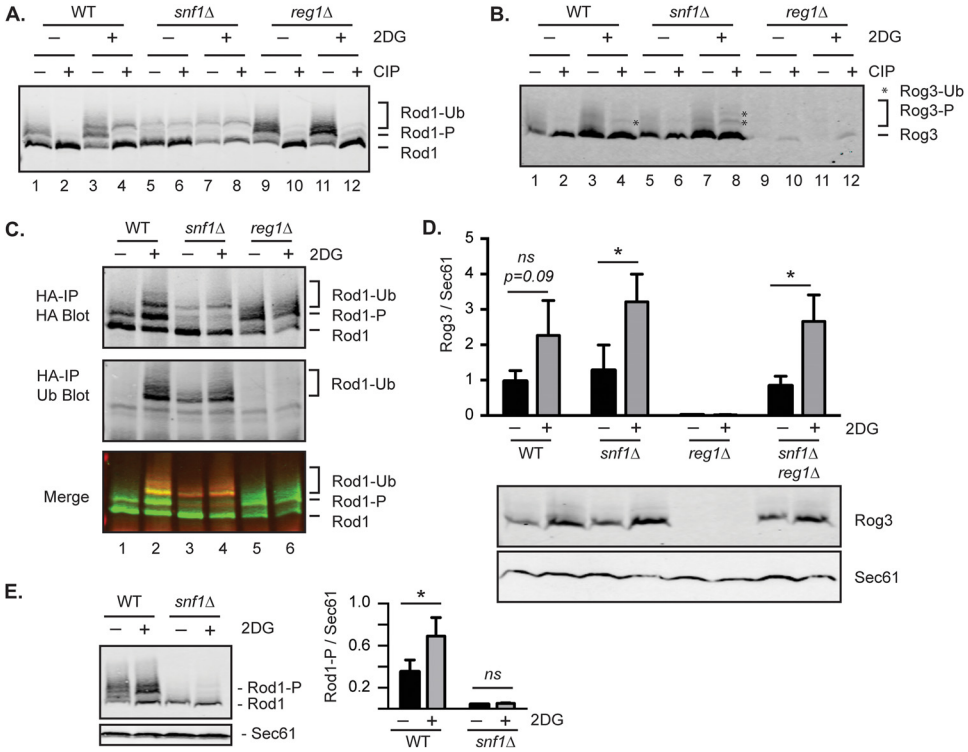

FIG 8 Posttranslational modifications of Rod1 and Rog3 in response to 2DG. (A and B) Cultures of wild-type, *snf1*Δ, or *reg1*Δ cells expressing either Rod1-3×HA (A) or Rog3-3×HA (B) were grown to mid-log phase and then were either left untreated or treated with 0.2% 2DG for 2 h. Protein extracts were incubated with or without calf intestinal alkaline phosphatase (CIP) prior to immunoblotting. Rod1-P, phosphorylated Rod1; Rod1-Ub, ubiquitinated Rod1. Asterisks indicate the CIP-resistant, slower-migrating bands of Rog3 that likely represent the Rog3-Ub species. (C) (Top and center) Rod1-3×HA immunoprecipitated (IP) with anti-HA antibodies was examined by immunoblotting with antiubiquitin and anti-HA antibodies. (Bottom) Merged image with overlapping signals shown in yellow. (D) The abundance of Rog3-3×HA protein was examined in cells of the indicated genotypes that were either left untreated or treated with 0.2% 2DG. The abundance of Rog3 was normalized to that of Sec61, and the mean ratios from triplicate samples ± standard errors were plotted. Representative blots are shown below the graph. (E) The phosphorylation of Rod1-3×HA protein was examined in wild-type and *snf1*Δ cells either left untreated or treated with 0.2% 2DG. The abundance of Rod1-P was normalized to that of Sec61, and the mean ratios from triplicate samples ± standard errors were plotted. Representative blots are shown on the left of the graph. *, $P < 0.05$; ns, $P > 0.05$.

cargo pairs, ubiquitination of the α-arrestins is required for their endocytic function (38, 40, 45, 67). Rod1 ubiquitination has been mapped to 4 lysine residues within the arrestin domain, which are perfectly conserved in Rog3 (Fig. 7A) (38, 67). When these residues in Rod1 are mutated to arginine, the resulting Rod1(4KR) mutant is able to bind Rsp5 but is no longer ubiquitinated (38, 67). In contrast to the requirement for Rsp5 binding, *rod1-4KR* and *rog3-4KR* behaved as hypomorphic alleles. While Rod1-4KR stimulated some vacuolar trafficking of Hxt1 and Hxt3 in response to 2DG, PM fluorescence was retained to a greater degree than was observed with wild-type Rod1 (Fig. 7D). Supporting the idea that Hxt1 and Hxt3 are retained at the PM, cells expressing Rod1-4KR displayed greater 2DG resistance than cells expressing wild-type Rod1 (Fig. 7B). Similarly, Rog3-4KR also conferred a somewhat higher degree of 2DG resistance than wild-type Rog3 (Fig. 7B); however, no discernible difference in Hxt localization was apparent (Fig. 7D). Thus, recruitment of Rsp5 is necessary and sufficient for Rod1 to promote the endocytosis of Hxt1 and Hxt3, presumably by ubiquitinating these transporters, but the α-arrestins themselves need not be ubiquitinated at these four conserved lysine residues in order to promote glucose transporter trafficking.

Posttranslational modification of Rod1 and Rog3 is altered in response to 2DG. Considerable evidence indicates that α-arrestins are regulated by phosphorylation and ubiquitination (38, 40, 41, 43, 45, 61, 67, 74). Both Rod1 and Rog3 were detectably phosphorylated when they were extracted from wild-type cells growing on glucose, as judged by the presence of a slower-migrating band(s) that collapsed after treatment with calf intestinal alkaline phosphatase (CIP) (Fig. 8A and B, lanes 1 and 2). Upon 2DG addition, phosphorylated species increased and a new, CIP-resistant, slower-migrating band appeared for both Rod1 and Rog3 (Fig. 8A and B, lanes 1 and 3). Immunoprecipitation of HA-tagged Rod1 from wild-type cells before and after treatment with 2DG, followed by blotting with an antiubiquitin antibody, confirmed that the slowest-migrating bands were ubiquitinated Rod1 (Fig. 8C, lanes 1 and 2).

For Rod1 in both the absence and the presence of 2DG, the phosphorylated forms were largely eliminated in *snf1*Δ cells (Fig. 8A, lanes 5 to 8, and E) and were markedly increased in *reg1*Δ cells, in which Snf1 is hyperactive (58, 59) (Fig. 8A, lanes 9 to 12); thus, the 2DG-stimulated increase in Rod1 phosphorylation is largely Snf1 dependent. Rod1 itself may be a substrate of the Reg1-containing isoform of PP1 (38), and hence, the elevated modification of Rod1 observed in *reg1*Δ cells could be enhanced by inefficient dephosphorylation. The increase in Rod1 ubiquitination caused by 2DG was somewhat reduced in *snf1*Δ cells (Fig. 8A). However,

Downloaded from http://mcb.asm.org/ on February 22, 2015 by University of Pittsburgh HSLS

we noted that in contrast to the pattern in wild-type cells, Rod1 was detectably ubiquitinated in *snf1*Δ cells even in the absence of 2DG treatment, and conversely, Rod1 was not ubiquitinated in *reg1*Δ cells either in the absence or in the presence of 2DG (Fig. 8C). These data are most consistent with a role for Snf1-dependent phosphorylation in preventing Rod1 ubiquitination.

Rog3 phosphorylation was also enhanced by 2DG addition, although it was not clear if the phosphorylation was Snf1 dependent. The slower-migrating Rog3 species appeared as a diffuse smear rather than distinct bands, hindering analysis (Fig. 8B). Nonetheless, it is clear that Rog3 was phosphorylated, because CIP treatment collapsed most of the diffusely migrating species into the single fastest-migrating band. Moreover, a readily detectable, slower-migrating, CIP-resistant Rog3 band(s) (Fig. 8B, asterisks) appeared in wild-type or *snf1*Δ cells in response to 2DG treatment. Rog3 protein levels in cells were noticeably higher after 2DG treatment (Fig. 8B and D). In contrast to the effect on Rod1, the hyperactive Snf1 in *reg1*Δ cells caused a dramatic reduction in Rog3 abundance (Fig. 8B and D). Furthermore, Rog3 abundance is regulated by Snf1, since Rog3 levels were restored in a *reg1*Δ strain if Snf1 was absent (Fig. 8D). These results show that at some level (expression and/or protein stability), Rog3 is negatively regulated by Snf1. Thus, Rod1 and Rog3 appear to be subject to different regulatory inputs both before 2DG treatment and in response to 2DG, presumably allowing for physiologically appropriate fine-tuning of their combined activities.

DISCUSSION

Prior studies have proposed a number of explanations for 2DG-induced toxicity, including accumulation of 2-deoxyglucose-6-phosphate as a metabolic inhibitor of glycolysis, reduction of cellular ATP pools, elevation of NADH levels, accumulation of defects in cell wall biogenesis, and disruption of protein glycosylation (6, 11, 20, 75, 76). Here we have documented that 2DG also reduces the expression and cell surface abundance of two glucose transporters, Hxt1 and Hxt3. To our knowledge, our findings are the first demonstration that the trafficking of glucose transporters to the vacuole markedly increases in response to 2DG, and they help to explain the observation that 2DG acts as a glucose starvation mimetic (77). Our data indicate that in addition to acting as a competing and nonproductive glucose analog, 2DG severely limits glucose entry by dampening transcription and stimulating the removal of Hxt1 and Hxt3 from the PM. Together, these effects reveal how 2DG causes a failure to proliferate even when exogenous glucose is abundant.

In our study, we also elucidated the mechanism of the 2DG-induced trafficking of Hxt1 and Hxt3. 2DG-stimulated internalization of Hxt1 and Hxt3 requires the action of two trafficking adaptors, α-arrestins Rod1 and Rog3, which deliver the ubiquitin ligase Rsp5 to these two hexose transporters, ostensibly to stimulate their ubiquitination and thereby mark them for endocytic removal. Furthermore, our data indicate that the function of Rod1 is negatively regulated by Snf1-dependent phosphorylation. When 2DG is present, Snf1 activation helps to counteract the Rod1- and Rog3-mediated internalization of Hxt1 and Hxt3 in an attempt to maintain some degree of glucose uptake. Rog3 shares 38 to 41% sequence identity (depending on alignment gaps) over its length with Rod1 (40, 42). Indeed, in the regulation of at least one other cargo, the GPCR Ste2, Rod1 and Rog3 play semiredundant roles (67). However, our analyses revealed some previously unrecognized distinctions between these two α-arrestins. First, Rod1 seems to be the adaptor solely responsible for Hxt1 internalization in response to 2DG, while Hxt3 endocytosis in response to 2DG was fully ablated only by the absence of both Rod1 and Rog3. Second, we found that Rod1 is a target for Snf1-dependent phosphorylation in response to 2DG, in agreement with prior observations that Rod1 is phosphorylated in a Snf1-mediated manner when glucose is limiting (38, 62). While the role of Snf1 in Rog3 phosphorylation was less clear, Snf1 plays a critical role in regulating Rog3 abundance. Also, we found that one Snf1 phosphorylation site in Rod1 characterized by others (62) is clearly not sufficient to affect Rod1 activity on Hxt1 and Hxt3. Third, both Rod1 and Rog3 need to associate with Rsp5 in order to bring about Hxt internalization in response to 2DG.

We propose a model (Fig. 9A) whereby under glucose-rich growth conditions, Snf1 activity is low (7, 58) but nonetheless important for the efficient uptake and utilization of glucose. Under these conditions, Snf1 selectively phosphorylates Rod1 to inhibit Rod1-mediated turnover of Hxt1 and Hxt3, thereby maintaining high-capacity glucose transporter activity at the surface. This model is supported by our observations that (i) Rod1 is phosphorylated in a Snf1-dependent manner even in the presence of glucose; (ii) Hxt1 and Hxt3 internalization is increased in *snf1*Δ cells; and (iii) deletion of *ROD1* prevents the endocytosis of Hxt1 and Hxt3.

Rod1 regulation of Hxt trafficking is controlled by a variety of posttranslational modifications (Fig. 9B). In the absence of Snf1 or when 2DG is added to the growth medium, Rod1 ubiquitination is dramatically increased. 2DG activates Snf1 (7), promotes Rod1 phosphorylation and ubiquitination, and greatly stimulates the trafficking of Hxt1 and Hxt3 to the vacuole. These data suggest that Snf1-mediated phosphorylation may both inhibit and activate the Rod1-regulated trafficking of hexose transporters. We envision two possible regulatory models. (i) The degree of Snf1-mediated phosphorylation of Rod1 dictates the response. In glucose-grown cells, low-level Snf1 activity and the phosphorylation of Rod1 inhibit Rod1 ubiquitination and Rod1-mediated trafficking of hexose transporters. Increased Snf1 activity due to 2DG addition leads to hyperphosphorylation of Rod1, increased ubiquitination, and increased trafficking of Hxt1 and Hxt3 (Hxt1/3) to the vacuole. (ii) Alternatively, Snf1 phosphorylation of Rod1 is always inhibitory, but a yet-to-be-identified, counteracting regulatory element becomes more active and drives the Rod1 equilibrium toward the ubiquitinated and Rsp5-bound form, capable of stimulating the endocytosis of Hxt1 and Hxt3 (Fig. 9B). Indeed, Reg1 could serve as the counterbalance to Snf1 in the latter scenario. Reg1 interacts with Rod1 and reduces Rod1 phosphorylation (38), in agreement with the observed hyperphosphorylation and lack of ubiquitination of Rod1 in the absence of Reg1. However, the elucidation of the role of Reg1 in controlling the α-arrestin-mediated trafficking of hexose transporters in response to 2DG is somewhat confounded by the fact that in the absence of Reg1, neither Hxt1 nor Hxt3 is well expressed. It is clear that Reg1 stimulates Rod1 dephosphorylation, either directly (by targeting the Glc7 phosphatase to Rod1), indirectly (by downmodulating Snf1 itself), or both. Rod1 is not detectably ubiquitinated in *reg1*Δ cells, suggesting that hyperphosphorylation of Rod1 inhibits its recruitment of Rsp5 and/or its ubiquitination, as has been proposed previously (38).

Rod1 ubiquitination, and likely Rog3 ubiquitination, was in-

Downloaded from http://mcb.asm.org/ on February 22, 2015 by University of Pittsburgh HSLS

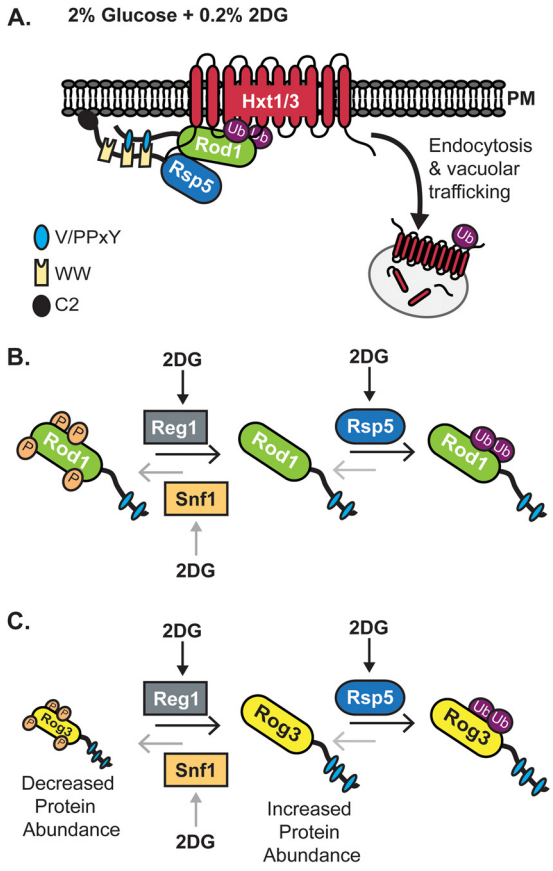

FIG 9 Model for α-arrestin-mediated regulation of hexose transporter abundance and localization. (A) In response to 2DG, Rod1 ubiquitination increases, suggesting increased binding between Rod1 and Rsp5 through their respective PPXY motifs and WW domains. Rsp5 membrane association is mediated by the Ca^{2+}-dependent lipid/protein binding (C2) domain. The Rod1-Rsp5 complex directs the ubiquitination and endocytosis of Hxt1/3. Hxt1/3 are subsequently trafficked to the vacuole, where they are degraded. (B) Rod1 regulation and posttranslational modifications. In response to 2DG, Snf1 is modestly activated and Rod1 phosphorylation increases (gray arrows). Under high-glucose conditions, the phosphorylation of Rod1 by Snf1 inhibits its trafficking function. In response to 2DG, Rod1 ubiquitination increases, promoting the internalization of hexose transporters, suggesting that an alternative, Snf1-counterbalancing pathway, such as the Reg1/Glc7 phosphatase, must also be activated by 2DG (black arrows). (C) Rog3 regulation and posttranslational modifications. In response to 2DG, Rog3 protein levels, and possibly Rog3 ubiquitination, are increased. In the absence of Reg1, Snf1 kinase hyperactivation promotes Rog3 degradation.

creased following 2DG treatment. While Rod1 and Rog3 ubiquitination is important, it is not absolutely required for Rod1- or Rog3-mediated trafficking of Hxt1/3 to the vacuole. Mutation of the 4 lysine residues identified as the ubiquitination sites in Rod1 (38, 67) produced hypomorphic alleles with greater retention of Hxt1 and Hxt3 at the PM and increased resistance to 2DG. Our results are in marked contrast to earlier studies, which reported that these sites were required for Rod1-mediated endocytosis of the lactate permease Jen1 (38). In agreement with our findings, however, ubiquitination of Rod1 is not required for its function in Ste2 internalization (67).

Binding of Rsp5 by Rod1 is required for the internalization of Hxt1 and Hxt3 as well as for that of other PM targets that undergo Rod1-dependent internalization, including Jen1 (38) and Ste2 (67). Mutation of the PPXY motifs in Rod1 and Rog3 eliminated their ability to support the endocytosis of Hxt1 and Hxt3 in response to 2DG and failed to restore 2DG sensitivity to *rod1*Δ *rog3*Δ cells. In addition, Rsp5 activity is required for the 2DG-induced endocytosis of Hxt1 and Hxt3, in agreement with recent reports showing that Rsp5 is critical for the downregulation of Hxt1 and Hxt3 upon nutrient starvation (32, 33). Thus, it seems likely that in response to 2DG, α-arrestin recruitment of Rsp5 stimulates Hxt ubiquitination, endocytosis, and trafficking to the vacuole (Fig. 9A).

The internalization of other glucose transporters, such as the high-affinity glucose transporter Hxt6, is also regulated by Rod1, which is internalized upon a shift from raffinose to glucose (42). Although the regulatory cues here have not been defined, loss of Snf1-mediated inhibition of Rod1 is plausible because addition of glucose leads to reduced Snf1 activity (58). While Hxt6 internalization is mediated by Rod1 in response to the carbon source, another α-arrestin, Csr2/Art8, regulates Hxt6 endocytosis in response to cycloheximide stress (42). In accordance with some functional redundancy between Rod1 and Csr2, we observed weak restoration of Hxt1 and Hxt3 trafficking to the vacuole in *9Arr*Δ cells complemented with Csr2 (Fig. 5E). Also, Csr2 was implicated in studies of Hxt3 downregulation in response to a glucose-to-ethanol shift, whereas Rod1 made little contribution (and Rog3 was not tested) (33). The internalization of Hxt3 upon a shift to ethanol requires Ras2 and TORC1 but not Snf1 (33). Thus, it appears that different signaling cues dictate the activities of specific α-arrestins under distinctive nutrient conditions, thereby determining the PM residence times of particular hexose transporters (42).

Like Rod1, Rog3 required Rsp5 recruitment to mediate Hxt3 endocytosis and confer sensitivity to 2DG. Mutation of the (V/P)PXY motifs in Rog3, which are required for its binding to Rsp5 (67), completely eliminated the Rog3-dependent internalization of Hxt3 and failed to restore 2DG sensitivity to *rod1*Δ *rog3*Δ cells. As with Rod1, a Rog3 allele (*rog3-4KR*) was also hypomorphic, suggesting that ubiquitination of Rog3 may not be needed for its optimal function in Hxt3 trafficking (Fig. 9C). However, in several other respects, Rog3 exhibited a pattern of regulation in response to 2DG different from that displayed by Rod1. In contrast to Rod1, it is unclear if Rog3 is a Snf1 substrate. Rog3 is phosphorylated in glucose-grown cells and in response to 2DG addition, yet this phosphorylation does not appear to be dependent on Snf1. Interestingly, the abundance of Rog3 is under complex regulation; in response to 2DG, when Snf1 is modestly activated, Rog3 levels increase. In *reg1*Δ cells, when Snf1 is hyperactive, Rog3 is nearly undetectable. The low abundance of Rog3 in *reg1*Δ cells is due to the hyperactivation of Snf1, as evidenced by the fact that Rog3 levels were restored in *reg1*Δ *snf1*Δ cells. These results demonstrate that Rog3 expression and/or stability is controlled by Snf1.

It is tempting to speculate that Rog3 may be regulated in a fashion analogous to that of the mammalian α-arrestin TXNIP. In mammalian cells, TXNIP is required for the endocytosis of the glucose transporter GLUT1, and the phosphorylation of TXNIP by AMPK targets it for degradation, thereby preventing GLUT1 internalization (27). Moreover, when present, TXNIP somehow reduces the level of *GLUT1* mRNA (27). If Rog3 has a similar additional regulatory role, it might explain the changes in *HXT* expression that we observed in 2DG-treated and/or *reg1*Δ cells. However, 2DG treatment activates AMPK in mammalian cells,

Downloaded from http://mcb.asm.org/ on February 22, 2015 by University of Pittsburgh HSLS

leading to TXNIP degradation (27), whereas the hyperactivation of Snf1 observed in *reg1*Δ yeast cells promoted the loss of Rog3 accumulation. Hence, the analogy between TXNIP and Rog3 is imperfect.

As shown here and in recent related work (7), Snf1 has some activity under high-glucose conditions and exhibits substrate selectivity that defines an unexpected role for Snf1 in regulating the 2DG sensitivity of glucose-grown cells. Although Snf1 is definitely less active when cells are growing in a high-glucose medium than in a low-glucose medium (7, 58), the enzyme clearly retains physiologically important activity, because *snf1*Δ cells are more sensitive to 2DG than wild-type cells. In glucose-grown cells, a low level of T120 phosphorylation can be detected (7), and active Snf1 has been found in other studies of cells growing on glucose (58, 64, 78–80). Snf1 activity is required for resistance to 2DG, and its phosphorylation on T210 increases in response to 2DG addition (7). Likewise, mammalian AMPK is activated by 2DG (27), suggesting that yeast and mammals share a conserved 2DG stress response. Glucose starvation causes robust activation of Snf1 and hyperphosphorylation of the transcriptional repressor Mig1 (59, 81); in contrast, 2DG-induced activation of Snf1 is modest yet sufficient for the increased phosphorylation of Rod1 but not of Mig1 (7). These observations raise the possibility that distinct signaling cues modulate Snf1 activity selectively, directing Snf1 toward distinct substrates.

Our findings lead us to propose that instead of acting as a binary off-on regulator of its downstream effectors, Snf1 acts more as a cellular rheostat, responsive to even subtle changes in the energy state of the cell and able to fine-tune the cellular response by selectively targeting its activity to specific substrates. In support of this proposal, Snf1 is activated by sodium stress in glucose-grown cells and is required for the sodium stress response (82); however, Mig1 is not phosphorylated in response to sodium stress (79). The identity of the critical Snf1 substrate(s) for sodium stress response is not known. Thus, the degree to which Snf1 is activated, the specific isoform that is activated, and the localization of the activated kinase or the stimulus that triggers Snf1 activation may all play roles in dictating the substrates that Snf1 phosphorylates. The molecular details of this selective Snf1 targeting remain to be elucidated but will undoubtedly provide exciting new insights into critical control of cellular signaling.

ACKNOWLEDGMENTS

This work was supported by NIH R01 research grant GM46443 (to M.C.S.) and by NIH R01 research grant GM21841 and funds from the UC Berkeley Energy Biosciences Institute (to J.T.). A.F.O was supported by development funds from the Department of Cell Biology (University of Pittsburgh), as well as by NIH R01 research grants GM21841 (to J.T.), DA014204-11 (to A. Sorkin, University of Pittsburgh), and GM75061 (to J. L. Brodsky, University of Pittsburgh).

We gratefully acknowledge helpful discussions with members of the Brodsky laboratory, and we thank Adam Kwiatkowski (University of Pittsburgh) for the use of his confocal microscope, Hugh Pelham (LMB, MRC, Cambridge, United Kingdom) for the *9arr*Δ strain, Widmar Tanner (Universität Regensburg, Regensburg, Germany) for the Hxt1-GFP-expressing plasmid pVTU100, Chris Burd (Yale University) for the *rsp5-1* strain, George van der Merwe (University of Guelph, Guelph, Ontario, Canada) for the Hxt3-GFP *rsp5-1* strain, and Chris Alvaro (UC Berkeley) for plasmids expressing Rod1-3HA and Rog3-3HA.

REFERENCES

1. **Chu S, DeRisi J, Eisen M, Mulholland J, Botstein D, Brown PO, Herskowitz I.** 1998. The transcriptional program of sporulation in budding yeast. Science **282:**699–705. http://dx.doi.org/10.1126/science.282.5389.699.
2. **Gasch AP, Werner-Washburne M.** 2002. The genomics of yeast responses to environmental stress and starvation. Funct Integr Genomics **2:**181–192. http://dx.doi.org/10.1007/s10142-002-0058-2.
3. **Griffin TJ, Gygi SP, Ideker T, Rist B, Eng J, Hood L, Aebersold R.** 2002. Complementary profiling of gene expression at the transcriptome and proteome levels in *Saccharomyces cerevisiae*. Mol Cell Proteomics **1:**323–333. http://dx.doi.org/10.1074/mcp.M200001-MCP200.
4. **Hardwick JS, Kuruvilla FG, Tong JK, Shamji AF, Schreiber SL.** 1999. Rapamycin-modulated transcription defines the subset of nutrient-sensitive signaling pathways directly controlled by the Tor proteins. Proc Natl Acad Sci U S A **96:**14866–14870. http://dx.doi.org/10.1073/pnas.96.26.14866.
5. **Washburn MP, Koller A, Oshiro G, Ulaszek RR, Plouffe D, Deciu C, Winzeler E, Yates JR, III.** 2003. Protein pathway and complex clustering of correlated mRNA and protein expression analyses in *Saccharomyces cerevisiae*. Proc Natl Acad Sci U S A **100:**3107–3112. http://dx.doi.org/10.1073/pnas.0634629100.
6. **Kang HT, Hwang ES.** 2006. 2-Deoxyglucose: an anticancer and antiviral therapeutic, but not any more a low glucose mimetic. Life Sci **78:**1392–1399. http://dx.doi.org/10.1016/j.lfs.2005.07.001.
7. **McCartney RR, Chandrashekarappa DG, Zhang BB, Schmidt MC.** 2014. Genetic analysis of resistance and sensitivity to 2-deoxyglucose in *Saccharomyces cerevisiae*. Genetics **198:**635–646. http://dx.doi.org/10.1534/genetics.114.169060.
8. **Jaspers HT, van Steveninck J.** 1975. Transport-associated phosphorylation of 2-deoxy-D-glucose in *Saccharomyces fragilis*. Biochim Biophys Acta **406:**370–385. http://dx.doi.org/10.1016/0005-2736(75)90017-6.
9. **Lobo Z, Maitra PK.** 1977. Resistance to 2-deoxyglucose in yeast: a direct selection of mutants lacking glucose-phosphorylating enzymes. Mol Gen Genet **157:**297–300. http://dx.doi.org/10.1007/BF00268666.
10. **Pelicano H, Martin DS, Xu RH, Huang P.** 2006. Glycolysis inhibition for anticancer treatment. Oncogene **25:**4633–4646. http://dx.doi.org/10.1038/sj.onc.1209597.
11. **Biely P, Kratky Z, Kovarik J, Bauer S.** 1971. Effect of 2-deoxyglucose on cell wall formation in *Saccharomyces cerevisiae* and its relation to cell growth inhibition. J Bacteriol **107:**121–129.
12. **Kratky Z, Biely P, Bauer S.** 1975. Mechanism of 2-deoxy-D-glucose inhibition of cell-wall polysaccharide and glycoprotein biosyntheses in *Saccharomyces cerevisiae*. Eur J Biochem **54:**459–467. http://dx.doi.org/10.1111/j.1432-1033.1975.tb04157.x.
13. **Cay O, Radnell M, Jeppsson B, Ahren B, Bengmark S.** 1992. Inhibitory effect of 2-deoxy-D-glucose on liver tumor growth in rats. Cancer Res **52:**5794–5796.
14. **Dwarkanath BS, Zolzer F, Chandana S, Bauch T, Adhikari JS, Muller WU, Streffer C, Jain V.** 2001. Heterogeneity in 2-deoxy-D-glucose-induced modifications in energetics and radiation responses of human tumor cell lines. Int J Radiat Oncol Biol Phys **50:**1051–1061. http://dx.doi.org/10.1016/S0360-3016(01)01534-6.
15. **Kern KA, Norton JA.** 1987. Inhibition of established rat fibrosarcoma growth by the glucose antagonist 2-deoxy-D-glucose. Surgery **102:**380–385.
16. **Raez LE, Papadopoulos K, Ricart AD, Chiorean EG, Dipaola RS, Stein MN, Rocha Lima CM, Schlesselman JJ, Tolba K, Langmuir VK, Kroll S, Jung DT, Kurtoglu M, Rosenblatt J, Lampidis TJ.** 2013. A phase I dose-escalation trial of 2-deoxy-D-glucose alone or combined with docetaxel in patients with advanced solid tumors. Cancer Chemother Pharmacol **71:**523–530. http://dx.doi.org/10.1007/s00280-012-2045-1.
17. **Vander Heiden MG, Cantley LC, Thompson CB.** 2009. Understanding the Warburg effect: the metabolic requirements of cell proliferation. Science **324:**1029–1033. http://dx.doi.org/10.1126/science.1160809.
18. **Warburg O.** 1956. On respiratory impairment in cancer cells. Science **124:**269–270.
19. **Datema R, Schwarz RT.** 1979. Interference with glycosylation of glycoproteins. Inhibition of formation of lipid-linked oligosaccharides in vivo. Biochem J **184:**113–123.
20. **Karczmar GS, Arbeit JM, Toy BJ, Speder A, Weiner MW.** 1992. Selective

Downloaded from http://mcb.asm.org/ on February 22, 2015 by University of Pittsburgh HSLS

depletion of tumor ATP by 2-deoxyglucose and insulin, detected by ^{31}P magnetic resonance spectroscopy. Cancer Res **52:**71–76.
21. **Kurtoglu M, Gao N, Shang J, Maher JC, Lehrman MA, Wangpaichitr M, Savaraj N, Lane AN, Lampidis TJ.** 2007. Under normoxia, 2-deoxy-D-glucose elicits cell death in select tumor types not by inhibition of glycolysis but by interfering with N-linked glycosylation. Mol Cancer Ther **6:**3049–3058. http://dx.doi.org/10.1158/1535-7163.MCT-07-0310.
22. **Diaz-Ruiz R, Uribe-Carvajal S, Devin A, Rigoulet M.** 2009. Tumor cell energy metabolism and its common features with yeast metabolism. Biochim Biophys Acta **1796:**252–265. http://dx.doi.org/10.1016/j.bbcan.2009.07.003.
23. **Hardie DG, Ross FA, Hawley SA.** 2012. AMPK: a nutrient and energy sensor that maintains energy homeostasis. Nat Rev Mol Cell Biol **13:**251–262. http://dx.doi.org/10.1038/nrm3311.
24. **Mayer FV, Heath R, Underwood E, Sanders MJ, Carmena D, McCartney RR, Leiper FC, Xiao B, Jing C, Walker PA, Haire LF, Ogrodowicz R, Martin SR, Schmidt MC, Gamblin SJ, Carling D.** 2011. ADP regulates SNF1, the *Saccharomyces cerevisiae* homolog of AMP-activated protein kinase. Cell Metab **14:**707–714. http://dx.doi.org/10.1016/j.cmet.2011.09.009.
25. **Hedbacker K, Carlson M.** 2008. SNF1/AMPK pathways in yeast. Front Biosci **13:**2408–2420. http://dx.doi.org/10.2741/2854.
26. **Ben Sahra I, Laurent K, Giuliano S, Larbret F, Ponzio G, Gounon P, Le Marchand-Brustel Y, Giorgetti-Peraldi S, Cormont M, Bertolotto C, Deckert M, Auberger P, Tanti JF, Bost F.** 2010. Targeting cancer cell metabolism: the combination of metformin and 2-deoxyglucose induces p53-dependent apoptosis in prostate cancer cells. Cancer Res **70:**2465–2475. http://dx.doi.org/10.1158/0008-5472.CAN-09-2782.
27. **Wu N, Zheng B, Shaywitz A, Dagon Y, Tower C, Bellinger G, Shen CH, Wen J, Asara J, McGraw TE, Kahn BB, Cantley LC.** 2013. AMPK-dependent degradation of TXNIP upon energy stress leads to enhanced glucose uptake via GLUT1. Mol Cell **49:**1167–1175. http://dx.doi.org/10.1016/j.molcel.2013.01.035.
28. **Jones GM, Stalker J, Humphray S, West A, Cox T, Rogers J, Dunham I, Prelich G.** 2008. A systematic library for comprehensive overexpression screens in *Saccharomyces cerevisiae*. Nat Methods **5:**239–241. http://dx.doi.org/10.1038/nmeth.1181.
29. **Ozcan S, Johnston M.** 1995. Three different regulatory mechanisms enable yeast hexose transporter (HXT) genes to be induced by different levels of glucose. Mol Cell Biol **15:**1564–1572.
30. **Ozcan S, Johnston M.** 1999. Function and regulation of yeast hexose transporters. Microbiol Mol Biol Rev **63:**554–569.
31. **Reifenberger E, Freidel K, Ciriacy M.** 1995. Identification of novel HXT genes in *Saccharomyces cerevisiae* reveals the impact of individual hexose transporters on glycolytic flux. Mol Microbiol **16:**157–167. http://dx.doi.org/10.1111/j.1365-2958.1995.tb02400.x.
32. **Roy A, Kim YB, Cho KH, Kim JH.** 2014. Glucose starvation-induced turnover of the yeast glucose transporter Hxt1. Biochim Biophys Acta **1840:**2878–2885. http://dx.doi.org/10.1016/j.bbagen.2014.05.004.
33. **Snowdon C, van der Merwe G.** 2012. Regulation of Hxt3 and Hxt7 turnover converges on the Vid30 complex and requires inactivation of the Ras/cAMP/PKA pathway in *Saccharomyces cerevisiae*. PLoS One **7:**e50458. http://dx.doi.org/10.1371/journal.pone.0050458.
34. **Ingham RJ, Gish G, Pawson T.** 2004. The Nedd4 family of E3 ubiquitin ligases: functional diversity within a common modular architecture. Oncogene **23:**1972–1984. http://dx.doi.org/10.1038/sj.onc.1207436.
35. **Lauwers E, Erpapazoglou Z, Haguenauer-Tsapis R, Andre B.** 2010. The ubiquitin code of yeast permease trafficking. Trends Cell Biol **20:**196–204. http://dx.doi.org/10.1016/j.tcb.2010.01.004.
36. **MacGurn JA, Hsu PC, Emr SD.** 2012. Ubiquitin and membrane protein turnover: from cradle to grave. Annu Rev Biochem **81:**231–259. http://dx.doi.org/10.1146/annurev-biochem-060210-093619.
37. **Gupta R, Kus B, Fladd C, Wasmuth J, Tonikian R, Sidhu S, Krogan NJ, Parkinson J, Rotin D.** 2007. Ubiquitination screen using protein microarrays for comprehensive identification of Rsp5 substrates in yeast. Mol Syst Biol **3:**116. http://dx.doi.org/10.1038/msb4100159.
38. **Becuwe M, Vieira N, Lara D, Gomes-Rezende J, Soares-Cunha C, Casal M, Haguenauer-Tsapis R, Vincent O, Paiva S, Leon S.** 2012. A molecular switch on an arrestin-like protein relays glucose signaling to transporter endocytosis. J Cell Biol **196:**247–259. http://dx.doi.org/10.1083/jcb.201109113.
39. **Han SO, Kommaddi RP, Shenoy SK.** 2013. Distinct roles for β-arrestin2 and arrestin-domain-containing proteins in β_2 adrenergic receptor trafficking. EMBO Rep **14:**164–171. http://dx.doi.org/10.1038/embor.2012.187.
40. **Lin CH, MacGurn JA, Chu T, Stefan CJ, Emr SD.** 2008. Arrestin-related ubiquitin-ligase adaptors regulate endocytosis and protein turnover at the cell surface. Cell **135:**714–725. http://dx.doi.org/10.1016/j.cell.2008.09.025.
41. **MacGurn JA, Hsu PC, Smolka MB, Emr SD.** 2011. TORC1 regulates endocytosis via Npr1-mediated phosphoinhibition of a ubiquitin ligase adaptor. Cell **147:**1104–1117. http://dx.doi.org/10.1016/j.cell.2011.09.054.
42. **Nikko E, Pelham HR.** 2009. Arrestin-mediated endocytosis of yeast plasma membrane transporters. Traffic **10:**1856–1867. http://dx.doi.org/10.1111/j.1600-0854.2009.00990.x.
43. **O'Donnell AF, Huang L, Thorner J, Cyert MS.** 2013. A calcineurin-dependent switch controls the trafficking function of α-arrestin Aly1/Art6. J Biol Chem **288:**24063–24080. http://dx.doi.org/10.1074/jbc.M113.478511.
44. **Patwari P, Emilsson V, Schadt EE, Chutkow WA, Lee S, Marsili A, Zhang Y, Dobrin R, Cohen DE, Larsen PR, Zavacki AM, Fong LG, Young SG, Lee RT.** 2011. The arrestin domain-containing 3 protein regulates body mass and energy expenditure. Cell Metab **14:**671–683. http://dx.doi.org/10.1016/j.cmet.2011.08.011.
45. **Merhi A, Andre B.** 2012. Internal amino acids promote Gap1 permease ubiquitylation via TORC1/Npr1/14-3-3-dependent control of the Bul arrestin-like adaptors. Mol Cell Biol **32:**4510–4522. http://dx.doi.org/10.1128/MCB.00463-12.
46. **Nabhan JF, Pan H, Lu Q.** 2010. Arrestin domain-containing protein 3 recruits the NEDD4 E3 ligase to mediate ubiquitination of the β_2-adrenergic receptor. EMBO Rep **11:**605–611. http://dx.doi.org/10.1038/embor.2010.80.
47. **Crapeau M, Merhi A, Andre B.** 2014. Stress conditions promote yeast Gap1 permease ubiquitylation and down-regulation via the arrestin-like Bul and Aly proteins. J Biol Chem **289:**22103–22116. http://dx.doi.org/10.1074/jbc.M114.582320.
48. **Winzeler EA, Shoemaker DD, Astromoff A, Liang H, Anderson K, Andre B, Bangham R, Benito R, Boeke JD, Bussey H, Chu AM, Connelly C, Davis K, Dietrich F, Dow SW, El Bakkoury M, Foury F, Friend SH, Gentalen E, Giaever G, Hegemann JH, Jones T, Laub M, Liao H, Liebundguth N, Lockhart DJ, Lucau-Danila A, Lussier M, M'Rabet N, Menard P, Mittmann M, Pai C, Rebischung C, Revuelta JL, Riles L, Roberts CJ, Ross-MacDonald P, Scherens B, Snyder M, Sookhai-Mahadeo S, Storms RK, Véronneau S, Voet M, Volckaert G, Ward TR, Wysocki R, Yen GS, Yu K, Zimmermann K, Philippsen P, Johnston M, Davis RW.** 1999. Functional characterization of the *S. cerevisiae* genome by gene deletion and parallel analysis. Science **285:**901–906. http://dx.doi.org/10.1126/science.285.5429.901.
49. **Rose MD, Winston FM, Hieter P.** 1990. Methods in yeast genetics. Cold Spring Harbor Laboratory Press, Cold Spring Harbor, NY.
50. **Fisher CL, Pei GK.** 1997. Modification of a PCR-based site-directed mutagenesis method. Biotechniques **23:**570–571, 574.
51. **Zhang Y, Nijbroek G, Sullivan ML, McCracken AA, Watkins SC, Michaelis S, Brodsky JL.** 2001. Hsp70 molecular chaperone facilitates endoplasmic reticulum-associated protein degradation of cystic fibrosis transmembrane conductance regulator in yeast. Mol Biol Cell **12:**1303–1314. http://dx.doi.org/10.1091/mbc.12.5.1303.
52. **Rose M, Botstein D.** 1983. Construction and use of gene fusions to LacZ (beta-galactosidase) that are expressed in yeast. Methods Enzymol **101:**167–180. http://dx.doi.org/10.1016/0076-6879(83)01012-5.
53. **Vida TA, Emr SD.** 1995. A new vital stain for visualizing vacuolar membrane dynamics and endocytosis in yeast. J Cell Biol **128:**779–792. http://dx.doi.org/10.1083/jcb.128.5.779.
54. **Randez-Gil F, Blasco A, Prieto JA, Sanz P.** 1995. DOGR1 and DOGR2: two genes from *Saccharomyces cerevisiae* that confer 2-deoxyglucose resistance when overexpressed. Yeast **11:**1233–1240. http://dx.doi.org/10.1002/yea.320111303.
55. **Sanz P, Alms GR, Haystead TA, Carlson M.** 2000. Regulatory interactions between the Reg1-Glc7 protein phosphatase and the Snf1 protein kinase. Mol Cell Biol **20:**1321–1328. http://dx.doi.org/10.1128/MCB.20.4.1321-1328.2000.
56. **Tu J, Carlson M.** 1995. REG1 binds to protein phosphatase type 1 and regulates glucose repression in *Saccharomyces cerevisiae*. EMBO J **14:**5939–5946.
57. **Zhang Y, McCartney RR, Chandrashekarappa DG, Mangat S, Schmidt**

Downloaded from http://mcb.asm.org/ on February 22, 2015 by University of Pittsburgh HSLS

MC. 2011. Reg1 protein regulates phosphorylation of all three Snf1 isoforms but preferentially associates with the Gal83 isoform. Eukaryot Cell **10:**1628–1636. http://dx.doi.org/10.1128/EC.05176-11.
58. **McCartney RR, Schmidt MC.** 2001. Regulation of Snf1 kinase. Activation requires phosphorylation of threonine 210 by an upstream kinase as well as a distinct step mediated by the Snf4 subunit. J Biol Chem **276:**36460–36466. http://dx.doi.org/10.1074/jbc.M104418200.
59. **Treitel MA, Kuchin S, Carlson M.** 1998. Snf1 protein kinase regulates phosphorylation of the Mig1 repressor in *Saccharomyces cerevisiae*. Mol Cell Biol **18:**6273–6280.
60. **Ayscough KR, Stryker J, Pokala N, Sanders M, Crews P, Drubin DG.** 1997. High rates of actin filament turnover in budding yeast and roles for actin in establishment and maintenance of cell polarity revealed using the actin inhibitor latrunculin-A. J Cell Biol **137:**399–416. http://dx.doi.org/10.1083/jcb.137.2.399.
61. **O'Donnell AF, Apffel A, Gardner RG, Cyert MS.** 2010. Alpha-arrestins Aly1 and Aly2 regulate intracellular trafficking in response to nutrient signaling. Mol Biol Cell **21:**3552–3566. http://dx.doi.org/10.1091/mbc.E10-07-0636.
62. **Shinoda J, Kikuchi Y.** 2007. Rod1, an arrestin-related protein, is phosphorylated by Snf1-kinase in *Saccharomyces cerevisiae*. Biochem Biophys Res Commun **364:**258–263. http://dx.doi.org/10.1016/j.bbrc.2007.09.134.
63. **Albuquerque CP, Smolka MB, Payne SH, Bafna V, Eng J, Zhou H.** 2008. A multidimensional chromatography technology for in-depth phosphoproteome analysis. Mol Cell Proteomics **7:**1389–1396. http://dx.doi.org/10.1074/mcp.M700468-MCP200.
64. **Braun KA, Vaga S, Dombek KM, Fang F, Palmisano S, Aebersold R, Young ET.** 2014. Phosphoproteomic analysis identifies proteins involved in transcription-coupled mRNA decay as targets of Snf1 signaling. Sci Signal **7:**ra64. http://dx.doi.org/10.1126/scisignal.2005000.
65. **Holt LJ, Tuch BB, Villen J, Johnson AD, Gygi SP, Morgan DO.** 2009. Global analysis of Cdk1 substrate phosphorylation sites provides insights into evolution. Science **325:**1682–1686. http://dx.doi.org/10.1126/science.1172867.
66. **Schreiber TB, Mausbacher N, Soroka J, Wandinger SK, Buchner J, Daub H.** 2012. Global analysis of phosphoproteome regulation by the Ser/Thr phosphatase Ppt1 in *Saccharomyces cerevisiae*. J Proteome Res **11:**2397–2408. http://dx.doi.org/10.1021/pr201134p.
67. **Alvaro CG, O'Donnell AF, Prosser DC, Augustine AA, Goldman A, Brodsky JL, Cyert MS, Wendland B, Thorner J.** 2014. Specific α-arrestins negatively regulate *Saccharomyces cerevisiae* pheromone response by down-modulating the G-protein coupled receptor Ste2. Mol Cell Biol **34:**2660–2681. http://dx.doi.org/10.1128/MCB.00230-14.
68. **Roy J, Cyert MS.** 2009. Cracking the phosphatase code: docking interactions determine substrate specificity. Sci Signal **2:**re9. http://dx.doi.org/10.1126/scisignal.2100re9.
69. **Shearwin-Whyatt L, Dalton HE, Foot N, Kumar S.** 2006. Regulation of functional diversity within the Nedd4 family by accessory and adaptor proteins. Bioessays **28:**617–628. http://dx.doi.org/10.1002/bies.20422.
70. **Dunn R, Hicke L.** 2001. Multiple roles for Rsp5p-dependent ubiquitination at the internalization step of endocytosis. J Biol Chem **276:**25974–25981. http://dx.doi.org/10.1074/jbc.M104113200.
71. **Galan JM, Moreau V, Andre B, Volland C, Haguenauer-Tsapis R.** 1996. Ubiquitination mediated by the Npi1p/Rsp5p ubiquitin-protein ligase is required for endocytosis of the yeast uracil permease. J Biol Chem **271:**10946–10952. http://dx.doi.org/10.1074/jbc.271.18.10946.
72. **Hein C, Springael JY, Volland C, Haguenauer-Tsapis R, Andre B.** 1995. NPl1, an essential yeast gene involved in induced degradation of Gap1 and Fur4 permeases, encodes the Rsp5 ubiquitin-protein ligase. Mol Microbiol **18:**77–87. http://dx.doi.org/10.1111/j.1365-2958.1995.mmi_18010077.x.
73. **Springael JY, Andre B.** 1998. Nitrogen-regulated ubiquitination of the Gap1 permease of *Saccharomyces cerevisiae*. Mol Biol Cell **9:**1253–1263. http://dx.doi.org/10.1091/mbc.9.6.1253.
74. **O'Donnell AF.** 2012. The running of the Buls: control of permease trafficking by α-arrestins Bul1 and Bul2. Mol Cell Biol **32:**4506–4509. http://dx.doi.org/10.1128/MCB.01176-12.
75. **Johnson BF.** 1968. Lysis of yeast cell walls induced by 2-deoxyglucose at their sites of glucan synthesis. J Bacteriol **95:**1169–1172.
76. **Kurtoglu M, Maher JC, Lampidis TJ.** 2007. Differential toxic mechanisms of 2-deoxy-D-glucose versus 2-fluorodeoxy-D-glucose in hypoxic and normoxic tumor cells. Antioxid Redox Signal **9:**1383–1390. http://dx.doi.org/10.1089/ars.2007.1714.
77. **Kim MS, Park JY, Namkoong C, Jang PG, Ryu JW, Song HS, Yun JY, Namgoong IS, Ha J, Park IS, Lee IK, Viollet B, Youn JH, Lee HK, Lee KU.** 2004. Anti-obesity effects of alpha-lipoic acid mediated by suppression of hypothalamic AMP-activated protein kinase. Nat Med **10:**727–733. http://dx.doi.org/10.1038/nm1061.
78. **Bodenmiller B, Wanka S, Kraft C, Urban J, Campbell D, Pedrioli PG, Gerrits B, Picotti P, Lam H, Vitek O, Brusniak MY, Roschitzki B, Zhang C, Shokat KM, Schlapbach R, Colman-Lerner A, Nolan GP, Nesvizhskii AI, Peter M, Loewith R, von Mering C, Aebersold R.** 2010. Phosphoproteomic analysis reveals interconnected system-wide responses to perturbations of kinases and phosphatases in yeast. Sci Signal **3:**rs4. http://dx.doi.org/10.1126/scisignal.2001182.
79. **Ye T, Elbing K, Hohmann S.** 2008. The pathway by which the yeast protein kinase Snf1p controls acquisition of sodium tolerance is different from that mediating glucose regulation. Microbiology **154:**2814–2826. http://dx.doi.org/10.1099/mic.0.2008/020149-0.
80. **Cherkasova V, Qiu H, Hinnebusch AG.** 2010. Snf1 promotes phosphorylation of the alpha subunit of eukaryotic translation initiation factor 2 by activating Gcn2 and inhibiting phosphatases Glc7 and Sit4. Mol Cell Biol **30:**2862–2873. http://dx.doi.org/10.1128/MCB.00183-10.
81. **Smith FC, Davies SP, Wilson WA, Carling D, Hardie DG.** 1999. The SNF1 kinase complex from *Saccharomyces cerevisiae* phosphorylates the transcriptional repressor protein Mig1p in vitro at four sites within or near regulatory domain 1. FEBS Lett **453:**219–223. http://dx.doi.org/10.1016/S0014-5793(99)00725-5.
82. **Alepuz PM, Cunningham KW, Estruch F.** 1997. Glucose repression affects ion homeostasis in yeast through the regulation of the stress-activated ENA1 gene. Mol Microbiol **26:**91–98. http://dx.doi.org/10.1046/j.1365-2958.1997.5531917.x.
83. **Thompson JD, Gibson TJ, Higgins DG.** 2002. Multiple sequence alignment using ClustalW and ClustalX. Curr Protoc Bioinformatics **Chapter 2:**Unit 2.3. http://dx.doi.org/10.1002/0471250953.bi0203s00.
84. **Kelley LA, Sternberg MJ.** 2009. Protein structure prediction on the Web: a case study using the Phyre server. Nat Protoc **4:**363–371. http://dx.doi.org/10.1038/nprot.2009.2.
85. **Brachmann CB, Davies A, Cost GJ, Caputo E, Li J, Hieter P, Boeke JD.** 1998. Designer deletion strains derived from *Saccharomyces cerevisiae* S288C: a useful set of strains and plasmids for PCR-mediated gene disruption and other applications. Yeast **14:**115–132. http://dx.doi.org/10.1002/(SICI)1097-0061(19980130)14:2<115::AID-YEA204>3.0.CO;2-2.
86. **Malinska K, Malinsky J, Opekarova M, Tanner W.** 2003. Visualization of protein compartmentation within the plasma membrane of living yeast cells. Mol Biol Cell **14:**4427–4436. http://dx.doi.org/10.1091/mbc.E03-04-0221.

Downloaded from http://mcb.asm.org/ on February 22, 2015 by University of Pittsburgh HSLS